Numerical Analysis of Two-phase Flow Characteristics in the Oscillating Capillary Tube Heat Pipe
(진동 세관형 히트 파이프에 있어서 2 상유동 특성에 대한 수치 해석)

Advisor : Jong Soo Kim

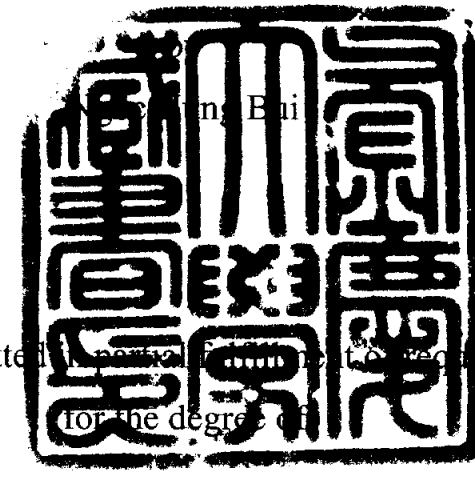

A thesis submitted in partial fulfillment of the requirements for the degree of

Doctor of Engineering

in the Department of Refrigeration and Air-Conditioning Engineering,
Graduate School, Pukyong National University

June 2003

Numerical Analysis of Two-phase Flow Characteristics in the Oscillating Capillary Tube Heat Pipe

A Dissertation

by

Ngoc Hung Bui

Approved as to style and content by :

Hoo-Kyu Oh
Chairman

Ki-Woo Lee
Member

Kyu-Il Han
Member

Eun-Pil Kim
Member

Jong-Soo Kim
Member

16 June, 2003

Contents

List of figures

List of tables

Numerical Analysis of Two-Phase Flow Characteristics in the Oscillating Capillary Tube Heat Pipe

Ngoc Hung Bui

Department of Refrigeration and Air-Conditioning Engineering, Graduate School, Pukyong National University

Abstract

진동세관형 히트파이프(OCHP) 내부에서 증기 기포들의 수축과 팽창에 의해서 길이 방향으로 진동되는 작동유체의 작동 방식을 유동 가시화 실험들을 통해 밝혔다. 수축과 팽창은 증발부와 응축부 각각에서 기포들의 형성과 소멸 때문에 일어난다. 실질적으로 물리적인 메커니즘을 보면, 각 채널에서의 진동과 순환등에 의해서 OCHP 는 복합적이면서도 불규칙적으로 열을 이동시킨다.

본 연구에서는 OCHP 의 작동메커니즘을 규명하기 위하여, 유동가시화를 통하여 밝혀진 유동양식을 근거로 2 개의 모델을 제안하였다. 첫 번째 모델은 균질 흐름에 기초하여 OCHP 에서 작동유체의 진동을 해석한 모델이며, 두 번째 모델은 두개의 액체 슬러그와 세 개의 기체 플러그로 분리된 모델에 기초하는 OCHP 의 분석적인 모델이다.

첫 번째 모델에서 이상류의 미분방정식이 적용되었고 동시에 비선형 편미분방정식이 풀어진다. 수치해석 결과 분석으로부터 OCHP 작동유체의 진동은 열흐름, 작동유체의 봉입량, 플로우 채널의 수력직경과 같은 작동조건이나 설계 상황에 영향을 받는다는 것을 알 수 있다.

두 개의 액 슬러그와 세 개의 증기 기포로 OCHP 를 단순화한 형상을 제안하였다. 증기 기포와 액 슬러그들의 유동을 예측하기 위해, 지배방정식을 세우고, 유한차분법을 이용해 풀었다. 결과들은 세관의 직경과 작동유체의 봉입량, 열유속 등이 OCHP 의 성능에 큰 영향을 미친다는 것을 알 수 있다.

시뮬레이션 결과들은 제안된 2 개의 모델이 OCHP 의 작동 메커니즘을 평가하는 것에 유용함을 보여준다.

Nomenclatures

A	: tube cross sectional area	[m^2]
c_p	: specific heat at constant pressure	[J/kgK]
c_v	: specific heat at constant volume	[J/kgK]
d	: diameter	[m]
f	: friction coefficient	
F	: friction force per unit volume	[N/m^3]
g	: gravitational acceleration	[m/s^2]
G	: mass velocity	[kg/m^2s]
h	: specific enthalpy	[J/kg]
h	: heat transfer coefficient	[W/m^2K]
h_{fg}	: laten heat of vaporization	[J/kg]
k	: thermal conductivity	[W/mK]
L	: length	[m]
m	: mass	[kg]
$\dot{m}$	: mass flow rate	[kg/s]
n	: integer	
p	: pressure	[Pa]
q	: heat flux	[W/cm^2]
Q	: heat transfer rate	[W]
r	: radius	[m]
R	: gas constant	[J/kgK]
Re	: Reynolds number	
t	: time	[s]

T	: temperature	[K] or [°C]
u	: internal energy	[J/kg]
v	: specific volume	[m^3/kg]
V	: volume	[m^3]
ν	: velocity	[m/s]
x	: axial coordinate	[m]
X	: vapor quality	

Greek letters

α	: charging ratio of working fluid	[vol.%]
θ	: inclination angle, contact angle	[°]
μ	: dynamic viscosity	[kg/ms]
υ	: kinematic viscosity	[m^2/s]
ρ	: density	[kg/m^3]
σ	: surface tension	[N/m]
τ	: shear stress	[N/m^2]

Subscripts

c	: cooling
$cond$	: condensation
evp	: evaporation
f	: liquid
fg	: vapor-liquid
g	: gas
h	: heating
in	: inlet
l	: liquid slug

le : left end

out : outlet

re : right end

sat : saturated

v : vapor plug

w : wall

Chapter 1

Introduction

1.1 Backgrounds

Heat pipe is one of the effective heat transfer devices being used in electronic equipments. Heat pipes such as thermosyphon, wick-type heat pipe, micro heat pipe [1], and dream pipe [2] are the representative configurations that they have already been applied.

However, there are various parameters that put limitations on the operation of conventional heat pipes. The capillary limit is the most commonly encountered limitation in the operation of heat pipes. It occurs when the capillary pumping rate is not sufficient to provide enough liquid to the evaporating section. This is due to the fact that the sum of the liquid and vapor pressure drops exceeds the maximum capillary pressure that the wick can sustain [1]. The entrainment limit is due to the influence of the shear force because the liquid and vapor flow in opposite directions. The interaction between this countercurrent liquid and vapor flow and the viscous shear forces occurring at the liquid-vapor interface may inhibit the return of liquid to the evaporating section [3].

For the limitation of installation space in electronic equipments, the conventional heat pipes have to be made of small structure for compactness. However, the limitation of heat transfer due to the decrease of structure causes difficulty for manufacturing the conventional heat pipes. Micro heat pipe can be

used to solve this problem but it has a complex structure and small quantity of heat transfer area [4]. The dream pipe has higher heat transfer coefficient by the axial oscillation of working fluid. However, its effective thermal conductivity is still lower than the effective thermal conductivity of heat pipes with two-phase heat transfer of working fluid. Also, it needs a power source, which can produce vibration.

The above limits can overcome by using the oscillating capillary tube heat pipe. It has high heat removal rate and can be also used for cooling of power electronics [5] as well as using for low temperature waste heat recovery systems with high performance and low cost.

The oscillating capillary tube heat pipe (OCHP), which is a very promising heat transfer device, was proposed by Akachi for the first time [6]. In addition to its excellent heat transfer performance, it has a simple structure: in contrast with conventional heat pipes, there is no wick structure to return the condensed working fluid back to the evaporating section. The OCHP is made from a long continuous capillary tube bent into many turns of serpentine structure as shown in Fig. 1.1. The working fluid is charged into the OCHP. The diameter of the OCHP must be sufficiently small so that vapor plugs can be formed by capillary action. The OCHP is operated within a 0.1 ~ 5 mm inner diameter range. If the diameter is too large, the liquid and vapor phases will tend to stratify. The OCHP can operate successfully for all heating modes. Due to the effect of surface tension, the working fluid will arrange in slug-train units in the OCHP. The heat input, which is the driving force, increases the pressure of the vapor plugs in the evaporating section. In turn, this pressure increase will push neighboring vapor plugs and liquid slugs toward the condensing section, which is at a lower pressure. However, due to the continuous heating, small vapor bubbles formed by nucleate boiling grow and coalescence to become vapor plugs. The flow of vapor plugs and liquid slugs moves to the condensing section by pressure difference. The heat transfer

continuously occurs. As a result, the heat is transported from the evaporating section to the condensing section by means of axial oscillations and phase changes of working fluid in the OCHP [6 ~ 8].

Until now, the OCHP have been used in heat transfer related application for the cooling of electronic equipments and low temperature waste heat recovery. However, its working mechanism is not specified clearly and there are no reliable data or tools for designing the OCHP according to given cooling requirements.

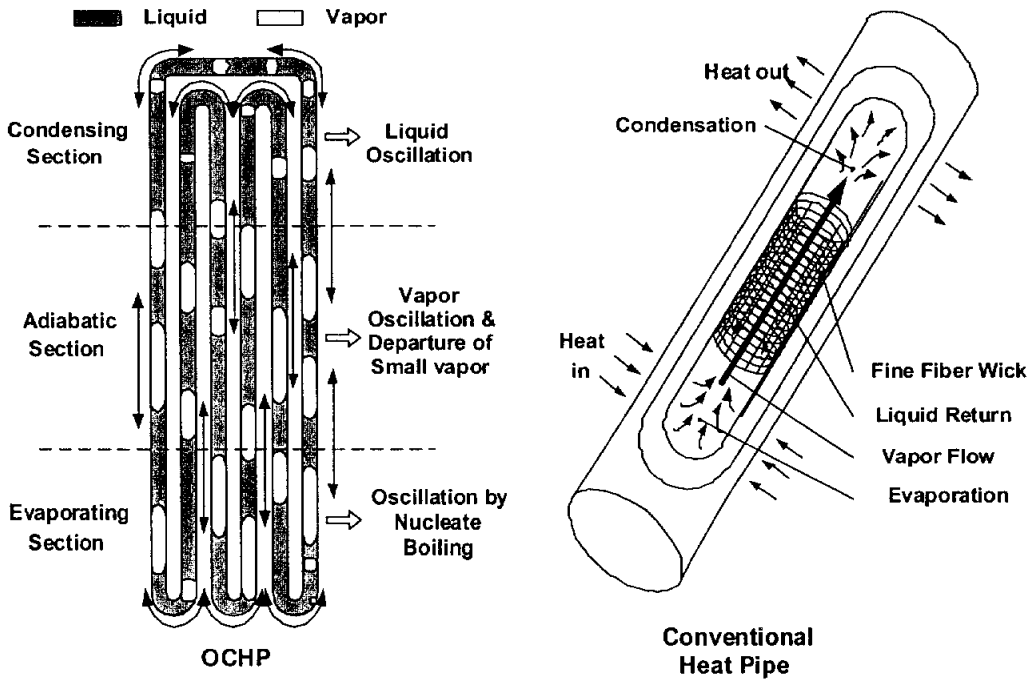

Fig. 1.1 Oscillating capillary tube heat pipe and conventional heat pipe

1.2 Review of previous studies

Both experimental and numerical investigations on the OCHP have been carried out by some researchers. The experiments mainly focus on examinations of flow pattern by flow visualization and heat transfer characteristics according to the design and operation conditions such as tube diameter, turn number, inclination angle, and the charging ratio of working fluid to find the optimal operation condition of the OCHP. And a few numerical investigations are developed to model the operating mechanism of the OCHP. However, these models are mostly based on rough assumptions and simplifications.

Takahashi et al. [9] conducted flow visualization experiments using the proton radiography method on the aluminum-extruded type OCHP. The cross section of flow channels was rectangular of 0.6 x 0.7 mm. The used working fluid was R-134a at the charging ratio of 30 vol.%. They concluded that the flow pattern depends on the inlet heat flux and inclination angle of the test section. However, in their study, the detailed flow pattern could not be understood by the indirectly projected flow pattern. So their experimental results only described the flow of vapor plugs and liquid slugs at each experimental condition.

Nishio et al. [10, 17, 21] compared the performance of the OCHP and dream pipe and proposed that the OCHP was more excellent in heat transfer performance than dream pipe. Nishio proposed the related equation to determine pipe diameter for the stable operation of the OCHP. They presented the special result that the OCHP of 2 turns was higher in effective thermal conductivity than that of 10 turns with glass pipes and water was used as working fluid. Furthermore, they also examined the influence of the charging ratio and inclination angle on effective thermal conductivity. They report that the heat transfer performance was high at the charging ratios of 30 ~ 50 vol. % and over inclination angles of 60 ~ 90°.

Hosoda et al. [11] estimated the heat transfer performance depending on the charging ratio of working liquid and heat flux. The OCHP of 10 turns was made of glass tubes (inner diameter of 2.4mm) and the used working fluid was distilled water. At the charging ratio of 60 vol.%, the maximal heat transfer performance was shown. They reported that the effective thermal conductivity at this condition was ten times even in glass pipe as well as in copper pipe.

Gi et al. [8, 13, 20] examined the heat transfer performance by experiments depending on the working temperature and the inclination angle of the OCHP. Teflon tubes (10 turns of 2 and 4 mm inner diameter) and copper tubes (40 turns of 1.6 and 2 mm inner diameter) were used. The used working fluid was R-142b. They reported that when the charging ratio was increased in the OCHP with teflon tubes, the vapor plugs were broke out and only liquid phase existed. As the operation temperature was high, short liquid and short vapor plugs were distributed within the OCHP. In the OCHP with copper tube, the effective thermal conductivity decreased by increasing the working temperature. When the tube diameter was decreased, the effective thermal conductivity increased. The heat transfer rate was the best with the charging ratios from 50 to 60 vol.% and the circulation velocity increased with increasing of the inclination angle of the OCHP.

Numata et al. [12] investigated flow visualization experiments according to the variation of tube diameter. The glass tube type OCHPs (of 2.4mm and 5mm inner diameters) were used and the working fluids were water and R-141b. They concluded that as the tube diameter was increased, the flow pattern changed from slug flow to churn flow and annular flow. However, the experimental results obtained in their study were somewhat different from the flow pattern in real metal tube because the glass tubes of low thermal conductivity were used. And the detailed flow pattern was not observed.

Miyazaki et al. [16, 23] implemented heat transfer experiments depending on the charging ratio and heating modes (bottom heat mode, horizontal heat mode and top heat mode) of the OCHP. The used working fluid was R-142b. The loop type OCHP of 25 channels (with rectangular cross section of 1.0 mm x 1.5 mm on a copper plate) and the loop type OCHP of 30 turns (made of copper pipes with inner diameter of 1 mm) were used. They observed the movement phenomena of oscillation wave of long liquid and vapor plugs and proposed an analytical model based on these phenomena. They concluded that the temperature oscillation depending on each heating mode was high in turn at bottom heat mode, horizontal heat mode and top heat mode. Also there exists an optimal value for the charging ratio, at which the heat transfer performance becomes maximal.

Kim and Lee et al. [14, 15] conducted flow visualization experiments according to the heat flux, charging ratio, and inclination angle of the OCHP. The OCHP consisted of a meandering closed structure (4 turns and 10 turns) with rectangular cross section of 1.5 x 1.5 mm machined into a brass plate. The used working fluid was ethanol and R-142b. The detailed flow pattern data were recorded by a high-speed digital camera to each experimental condition. They concluded that the oscillation of vapor bubbles caused by nucleate boiling and vapor oscillation and the departure of small bubbles are considered as the representative flow patterns at the evaporating section and at the adiabatic section, respectively.

Nagata et al. [18, 22] researched the influence of the working fluid (water, ethanol, R-141b) on the heat transfer performance using glass pipes of 2.4 mm inner diameter called bubble-driven heat transport tubes. They concluded that the working fluid with small capillary force had more stable working. The capillary force in the OCHP depends on surface tension, density, tube diameter and contact angle (with the inner surface of tube). They also reported that the self-excited oscillation of liquid columns might occur if the number of turns was reduced. And

the effective thermal conductivity of the OCHP could be increased when the turn number was reduced. The self-excited oscillation could be induced at the charging ratio of 75 vol.%. The effective thermal conductivity of the 2 ~ 4 turn OCHPs was much higher than that of the 10 ~ 20 turn OCHPs.

Maezawa et al. [19, 24, 25] analyzed the characteristics of temperature oscillations of working fluid by determinist method based on chaotic dynamics of data obtained from experiments. The OCHP of 40 turns was made of copper capillary tubes (inner diameters of 1 and 2 mm). Water and R-142b were used as the working fluids at the charging ratio of 40 vol.%. They analyzed oscillation phenomenon by chaotic behavior of the temperature oscillation characteristics of the working fluid. They also obtained the relation between heat flux and thermal resistance. They reported that the OCHP was operated by self-excited oscillation even though at the top heat mode. The thermal resistance was small in turn at top heat mode, horizontal heat mode and bottom heat mode. The temperature oscillation increased and variable frequency was higher at the same heat flux as the tube diameter got smaller. They also reported that when the tube diameter was decreased the high dimensional chaotic behavior was shown at low heat flux.

Kim and Lee et. al. [26, 27] investigated the heat transfer characteristics of the OCHP depending on the charging ratio and inclination angle. The used OCHP was a flat extruded aluminum tube of 2000 mm length, 18 mm width, 1.8 mm thickness and 8 shells (rectangular channel with cross section of 1.75 x 0.8 mm). R141b was used as the working fluid. They reported that the optimal operating condition, which has maximal heat transfer rate, obtained at the charging ratio of 40 vol.% and the inclination of 90°.

Table 1.1 Previous studies on heat transfer characteristics of the OCHP.

Author(s)	Working fluid	Test tube	Test conditions	Description
Takahashi et al. [9]	R-134a	Flat aluminum extruded tube I.D. : 0.6×0.7mm 15 turns	α = 30 *vol.*% θ = 90, 45, 0, 90^0	Flow pattern depend on heat flux and inclination angle
Nishio et al. [10, 17, 21]	Water	Glass tube I.D. : 2.4 mm 2 turns and 10 turns	α = 10 ~ 80 *vol.*% *at* 90^0 θ = 30 ~ 90^0 *at* 30 *vol.*%	Effective thermal conductivity Heat transfer rate
Hosoda et al. [11]	Water	Glass tube I.D. : 2.4 mm 10 turns	α = 20 ~ 70 *vol.*% θ = 90^0	Effective thermal conductivity
Gi et al. [8, 13, 20]	R-142b	Teflon tube I.D. : 2, 4 mm 10 turns	α = 30, 50, 70 *vol.*% *at* 30, 60, 90^0 θ = 30~90^0 *at* 30, 50, 70 *vol.*%	Average velocity of working fluid Heat transfer rate
		Copper tube I.D.: 2, 1.6 mm 40 turns	α = 40 *vol.*% θ = −90 ~ 90^0	Thermal resistance Effective thermal conductivity Heat transfer coefficient
		Copper tube I.D. : 2.0 mm 40 turns	α = 50 *vol.*% θ = −90 ~ 90^0	
Numata et al. [12]	Water R-141b	Glass tube I.D. : 2.4 and 5 mm 2 turns	α = 40 *vol.*% θ = 90^0	Flow pattern depend on tube diameter

Author(s)	Working fluid	Test tube	Test conditions	Description
Miyazaki et al. [16, 23]	R-142b	Copper plate I.D. : 1×1.5mm 25 turns	α = 42 *vol.*% $\theta = -15^0$	Oscillation wave of long liquid and vapor plugs & Temperature oscillation depending heating mode
		Copper tube I.D. : 1 mm 30 turns	α = 37,70 *vol.*% $\theta = 90^0$	
Kim and Lee et al. [14, 15, 26, 27]	Ethanol R-142b	Brass plate I.D.: 1.5×1.5 mm 4 turns 10 turns	$\alpha = 20 \sim 80$ *vol.*% θ = 30, 60, 90^0	Flow pattern Thermal resistance Effective thermal conductivity Heat transfer rate depend on heat flux, charging ratio and inclination angle
	R-141b	Aluminum flat extruded tube I.D.: 1.75×0.8 mm 4 turns	$\alpha = 20 \sim 70$ *vol.*% $\theta = 0 \sim 90^0$	
Nagata et al. [18, 22]	Water Ethanol R-141b	Glass tube I.D. : 2.4 mm 2 turns, 10 turns	$\alpha = 30 \sim 90$ *vol.*% $\theta = 90^0$	Effective thermal conductivity Heat transfer rate
Maezawa et al. [19, 24, 25]	Water R-142b	Copper tube I.D. : 1, 2 mm 40 turns	α = 40 *vol.*% θ = −90, 0, 90^0	Chaotic behavior of temperature oscillations Relation between heat flux and thermal resistance

Nagata et al. [22] analyzed the vapor plug propagation phenomenon by the one-dimensional homogeneous flow model. This phenomenon indicated that the self-excited oscillation of liquid columns might occur as the turn number was reduced. The effective thermal conductivity of the 2 ~ 4 turn OCHPs was much higher than that of the 10 ~ 20 turn OCHPs. They also reported that the surface temperature distribution and experimental result have similar trends. It depends on the position of outside wall surface of the OCHP.

Miyazaki et al. [28 ~ 30] proposed a theoretical model, which was strongly supported by experimental results, to predict the oscillatory flow characteristics of the OCHP. The wave equation from the relation of pressure and void fraction obtained in which reciprocal excitation between pressure and void fraction was assumed. They estimated the stability of pressure oscillation depending on the charging ratio of working fluid. Experimental examinations were made to compare the oscillation feature predicted by the analysis model with that of the experimental results. In experiments, two types of pressure oscillation were observed: the small and stable oscillation of symmetrical wave shape and the large oscillation having abrupt pressure change. It was seen from the examinations that the small oscillation seems to correspond to the predicted result. Their theoretical model could be used to estimate the pressure and displacement of oscillatory flow.

Maezawa et al. [31 ~ 33] presented studies, which propose the existence of chaos in the OCHP under some operating conditions. The approach in these studies is to analyze the time series of fluctuation of temperature of a specified location on the tube wall of the OCHP (adiabatic section) by power spectrum calculated through Fast Fourier Transform (FFT). The two dimensional mapping of the strange attractor and the subsequent calculation of the Lyapunov exponent have been done to prove the existence of chaos in the OCHP. A theoretical model on a single loop type of the OCHP has also been undertaken [33]. In this study basic equations of two-phase flow are applied to a single loop of the OCHP and it

is concluded that chaotic dynamics governs the flow over a wide range of heat transfer rates. While these studies have certainly added another dimension to the already complex behavior of the OCHP, the results should be judged cautiously because the frequency of temperature measurement extremely important for analyzing non-equilibrium behavior in the OCHP. Also, there should be more investigations of similar nature for further confirmation of the existence of chaotic phenomena in the OCHP.

Dobson et al. [34 ~ 37] have applied the governing equations of mass, momentum and energy to a simplified OCHP consisting of single liquid slug with vapor bubbles on both the sides as shown in Figure 1.2. The fundamental equations are applied to the vapor bubbles, the liquid thin film surrounding the bubbles, the tube and the liquid slug. They have also built an experimental setup for the validation of the model. It was found that the theoretical model does not give exact results of the movement of the liquid slug but only predicts the general tendencies of the liquid slug movement. The authors concluded that the initial length of the liquid slug, the thickness of the liquid slug and the interfacial mass flux have an influence on the movement of the liquid slug and it need to be better modeled to obtain more reasonable results.

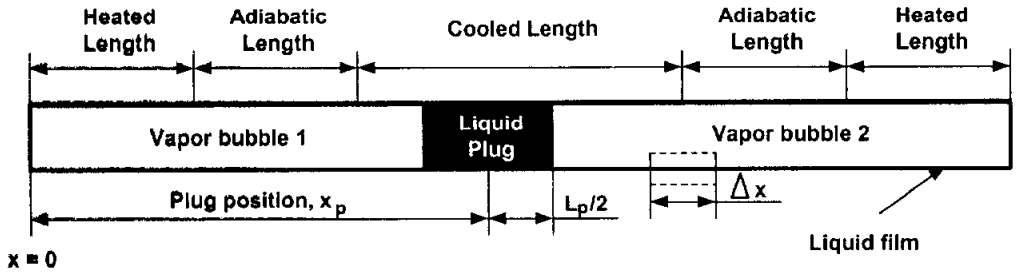

Fig. 1.2 Schematic of the model presented by Dobson et al.

Zuo et al. [38, 39] have tried to model the oscillation action of an OCHP by comparing the oscillation action of the OCHP to a single spring-mass-damper system represented by a second order homogeneous differential equation with time dependent spring constant. As can be seen from the proposed equation and its model in Fig. 1.3, the equation is quite similar to the governing equation for mechanical vibrations with viscous damping, except for the last term that is not only a function of x but also a function of t. They concluded that the fluid oscillation is sensitive to the charging ratio and the steady state of oscillation of the OCHP is obtained at the charging ratio of 75 vol.%. However, this oversimplified model has very limited applicability especially when compared to experimental results of flow patterns by visualization method.

$$\frac{d^2x}{dt^2}+\underbrace{\left(\frac{8\mu_f \pi d\alpha_0}{\rho_f dA}\right)\frac{dx}{dt}}_{\text{Viscous damping term}}+\underbrace{\frac{2A^2RT_{sat}}{\left(LA\rho_f\alpha_0\right)\left[(L/2)A\rho_f(1-\alpha_0)/\rho_g\right]^2}\left[(L/2)A\rho_f(1-\alpha_0)+\frac{Q_e}{h_{fg}}t\right]}_{\text{Spring stiffness term, } k(x,t)}x=0$$

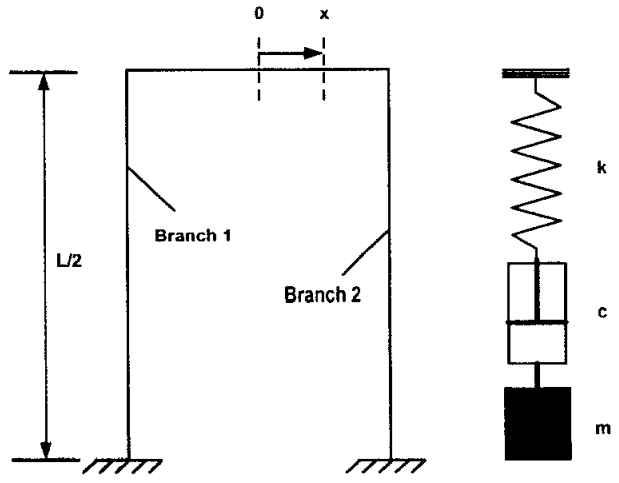

Fig. 1.3 Model with single spring mass damper system presented by Zuo et al.

The modeling approach presented by Wong et al. [40] is without any heat transfer considerations and only predicts the kinematics of the liquid-vapor slug system through the Lagrangian approach. In this case an open loop OCHP is modeled as shown in Fig. 1.4 under adiabatic conditions. The effect of sudden pressure pulse on the system is studied and the results of parametric analysis with respect to slug and plug lengths on pressure propagation are presented. While this approach can give important insights into the device operation, the oversimplifications cannot be ignored. It has been experimentally demonstrated that pressure waves and pressure pulses are simultaneously present in an OCHP with complex heat transfer implications.

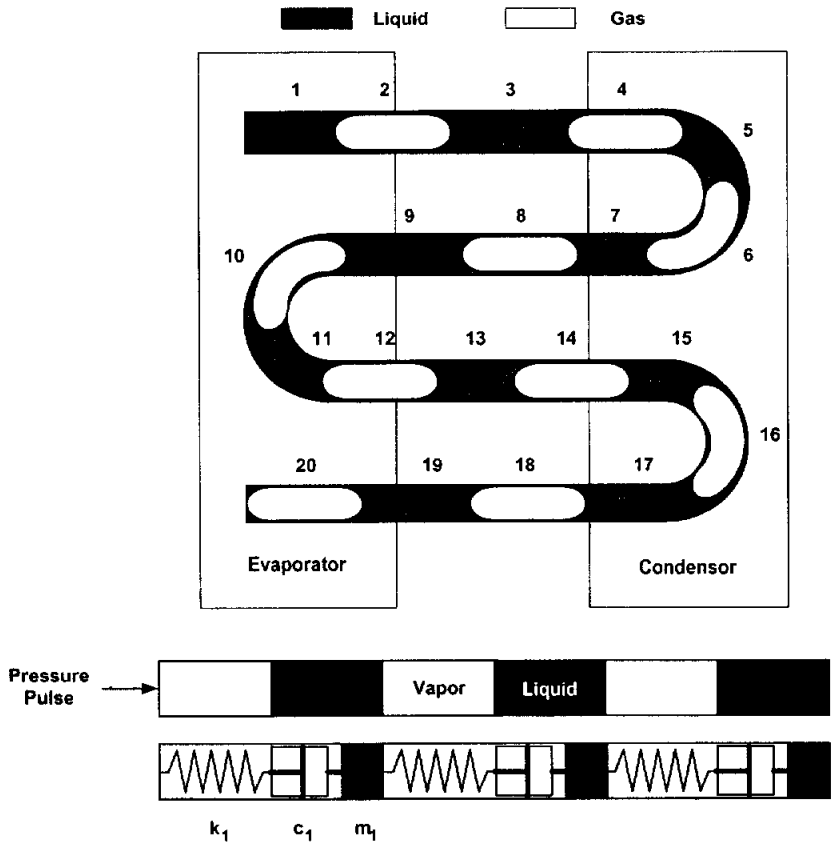

Fig. 1.4 Model with multiple spring mass system presented by Wong et al.

Table 1.2 Previous studies on numerical analysis of the OCHP.

Author(s)	Method	Assumption	Description
Nagata et al. [22]	One dimension homogeneous flow model	- Heat balance - Liquid heat transfer coefficient was taken as two phase heat transfer coefficient	Temperature distribution
Miyazaki et al. [28 ~ 30]	Self-excited model between pressure and void fraction	- Continuous distribution of void fraction in tube - Change of void fraction in a turn is neglected	Pressure oscillation & Wave velocity equation
Maezawa et al. [31 ~ 33]	One dimension model based on the existence of chaotic dynamics	- Flow model is homogeneous and non-slip two phase flow	Fluctuation of temperature Attractor map Power spectrum
Dobson et al. [34 ~ 37]	One dimension oscillatory model by explicit finite difference scheme	- Incompressible liquid - Ideal gas	Movement of liquid slug with different initial conditions
Zuo et al. [38, 39]	An equivalent single spring-mass-damper system	- The fluid oscillation is represented by the motion of the center-of-mass point of the fluid	Working fluid oscillation
Wong et al. [40]	One dimension model based on Lagrangian approach	- Adiabatic condition - Incompressible liquid - Ideal gas - No gravitational effect	Pressure Velocity

Mathematical modeling and theoretical analysis of the OCHP has been attempted in the recent past with many simplified approaches. The models may be summarized according to the adopted simplification scheme as the followings.

1. The oscillation wave inside the OCHP is predicted as the relation of pressure oscillation and void fraction [28 ~ 30].

2. Mathematical analysis of the OCHP is done highlighting the existence of chaos under some operating conditions. [31 ~ 33]

3. The movement of working fluid inside the OCHP is modeled by applying fundamental equations of mass, momentum and energy to specified control volume [34 ~ 37].

4. The oscillation action of the OCHP is compared to an equivalent single spring-mass-damper system in which the system specifications are affected by the heat transfer [38, 39].

5. In a similar approach as above, instead of single spring-mass-damper system, the OCHP is compared to a multiple spring-mass-damper system. This model describes only the kinematics of the liquid-vapor slugs without considering any heat transfer characteristics [40].

In this study, two simplified models of the OCHP were presented. The first model based on the homogeneous flow model was developed to model the oscillating motion of working fluid in the OCHP. The differential equations of two-phase flow were applied and simultaneous non-linear partial differential equations were solved. From the analysis of the numerical results, it was found that the oscillating motion of working fluid in the OCHP was affected by the operation and design conditions such as the heat flux, the charging ratio of working fluid and the hydraulic diameter of flow channel. The simulation results

showed that the proposed model and solution could be used for estimating the operating mechanism in the OCHP.

The second model was an analytical model of the OCHP based on the separated flow model with two liquid slugs and three vapor plugs. The governing equations were solved using an explicit finite difference scheme to predict the behavior of vapor plugs and liquid slugs. The results show that the diameter, surface tension, and charge ratio of working fluid have significant effects on the performance of the OCHP.

1.3 Objectives and Outline of the present study

The investigations on the operating mechanism of the OCHP using visualization method revealed that the working fluid in the OCHP oscillated to the axial direction by the contraction and expansion of vapor plugs. The contraction and the expansion were due to the formation and extinction of bubbles in the evaporating section and condensing section, respectively. The actual physical mechanism, whereby heat was transferred in the OCHP was complex and not well understood.

There were two simplified models of the OCHP presented in this study. The first model based on the homogeneous flow model was developed to model the oscillating motion of working fluid in the OCHP. The second was an analytical model of the OCHP based on the separated flow model with two liquid slugs and three vapor plugs. The governing equations were solved to predict the behaviors of the two-phase flow in two models. From the analysis of the numerical results, it was found that the oscillating motion of working fluid in the OCHP was affected by the operation and design conditions such as the heat flux, the charging ratio of working fluid and the hydraulic diameter of flow channel. The numerical results also showed that the proposed models and solution could be used for estimating

the operating mechanism in the OCHP.

This thesis included five chapters, which were summarized as follows:

- Chapter 1 showed the backgrounds of the present study by introduction the history of development of the OCHP and the previous investigations on the OCHP. The primary previous studies were summarized. Finally, the outline of the present study was presented.

- Chapter 2 presented the theory analysis of the present study by analyzing the working principle of the OCHP. The fundamental processes of the OCHP such as the heat and mass transfer processes, the effect of the type and the turn number of the OCHP were also investigated in this chapter.

- Chapter 3 presented the first model of the OCHP based on the homogeneous flow model. The differential equations of the two-phase flow were applied and simultaneous non-linear partial differential equations were solved. From the analysis of the numerical results, it was found that the oscillating motion of working fluid in the OCHP was affected by the operation and design conditions such as the heat flux, the charging ratio of working fluid, and the hydraulic diameter of flow channel.

- Chapter 4 presented the second model of the OCHP based on the separated flow model. The model was an analytical model of the OCHP with two liquid slugs and three vapor plugs. The governing equations were solved using an explicit finite difference scheme to predict the behavior of vapor plugs and liquid slugs. The numerical results showed that the diameter, surface tension, and charging ratio of working fluid had significant effects on the performance of the OCHP.

- Chapter 5 summarized the previous chapters and showed the final conclusions and future works.

Chapter 2

The working principle of the OCHP

2.1 The flow pattern in working process

The OCHP was first evacuated then filled with working fluid. It was observed that liquid slugs and vapor plugs were randomly distributed in the OCHP. Figure 2.1 shows the co-existence of liquid slugs and vapor plugs of different lengths in their initial condition in the OCHP, which was placed at the vertical orientation, before heat was applied. When OCHP was placed in the horizontal orientation, a similar arrangement of liquid slugs and vapor plugs was also observed. This was due to the fact that the surface tension was dominant over the gravitation force. This kind of capillary slug flow was a representative flow pattern in the operation process of the OCHP. As mentioned in chapter 1, Akachi et al. [6] reported that the flow pattern of liquid and vapor in the OCHP was formed to liquid slug and vapor plug shapes and they were distributed irregularly within the tube (of a 0.1 ~ 5 mm inner diameter). Rossi et al. [41] also concluded that this flow pattern existed within a 0.1 ~ 3 mm inner diameter range. However, these conditions could somewhat differ to the cross section of flow channel, the slip ratio of liquid and vapor, and the properties of working fluid. The flow patterns such as

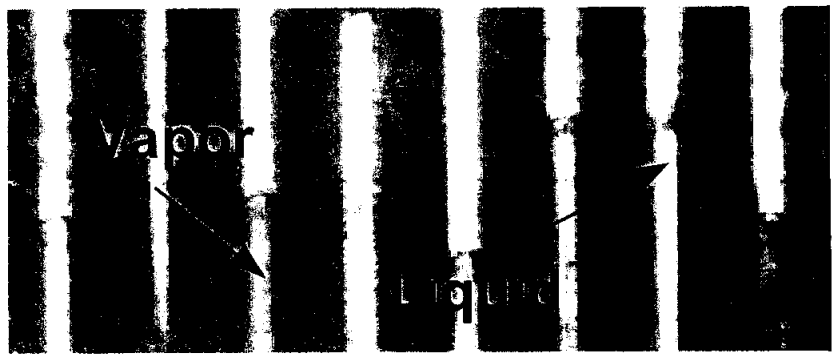

Fig. 2.1 Capillary slug flow [27]

dispersed flow (bubble flow, mist flow), annular flow, churn flow, and wavy flow as well as capillary slug flow are the general flow patterns in the capillary tube of a 1 ~ 5 mm inner diameter range [42 ~ 47].

When heat, which was the driving force, was applied to the evaporating section of the OCHP, the pressure of vapor plugs in the evaporating section increased. In turn, this pressure increase pushed neighboring vapor plugs and liquid slugs toward the condensing section, which was at a lower pressure. However, due to the continuous heating, small vapor bubbles formed by nucleate boiling grew and coalesced to become vapor plugs. The flow of vapor plugs and liquid slugs moved to the condensing section by pressure difference. The condensation of vapor plugs continuously occurred in the condensing section. As a result, thermal energy was rapidly transferred from the evaporating section to the condensing section as well as the oscillation and circulation of liquid slugs and vapor plugs occurred in the OCHP [6, 7].

Figure 2.2 shows the flow patterns at the steady state operation of the OCHP when the charging ratio was 40 vol.%. At the evaporating section, bubbles were continuously generated on the walls of the channels. These bubbles coalesced to become vapor plugs and the active oscillation phenomenon occurred. At the

adiabatic section, the flow pattern was divided into the liquid and vapor phase to the axial direction. The oscillation of liquid slugs and vapor plugs occurred very actively. When long vapor plugs and liquid slugs oscillated to the axial direction, the top part of these vapor plugs was separated to generate short vapor plugs. The flow pattern in the adiabatic section changed to the flow of short vapor-liquid slug-train units. At the condensing section, some short vapor plugs reduced in size and disappeared by the condensing process [48].

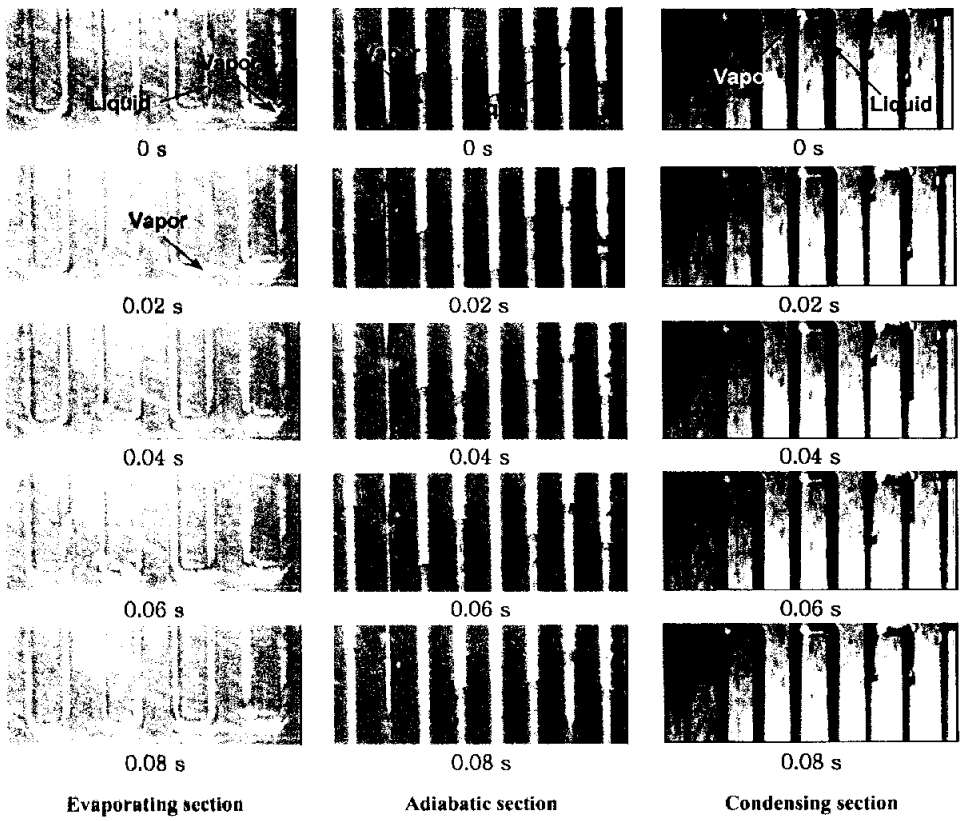

Fig. 2.2 Flow visualization at each section of the OCHP [48]

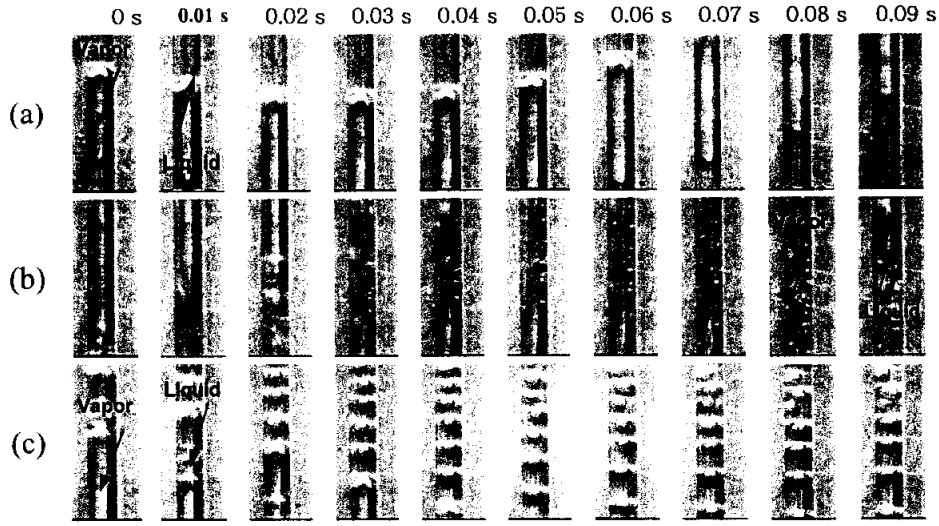

Fig. 2.3 Flow visualization at a flow channel of the OCHP [48]

Figure 2.3 shows the enlarged photographs at a flow channel of the OCHP. The capillary slug flow at a local point of the evaporating section near the adiabatic section is represented in Fig. 2.3(a). The oscillation of a long vapor plug and liquid slug was confirmed when condensed liquid was sufficiently supplied to the evaporating section. Fig. 2.3(b) shows the generation process of small bubbles by nucleate boiling at the liquid film (between the vapor plug and channel walls) when the oscillation of the liquid slugs and vapor plugs inside flow channels of the OCHP was active. Fig. 2.3(c) shows results for the case when bubble size was reduced by the compression operation of the ascending vapor plugs (at the bottom of the evaporating section) and the liquid slugs descending (from the condensing section) [48].

Generally, the flow pattern in the OCHP was observed as the separated flow (of liquid slugs and vapor plugs) and the homogeneous flow of bubbles generated inside liquid slugs and the thin liquid film [48]. Therefore, there were two simplified models of the OCHP presented in this study. The first model based on

the homogeneous flow model was developed to model the oscillating motion of working fluid with bubbles generated inside liquid slugs and the thin liquid film. The oscillation of liquid slugs and vapor plugs was simulated by the second model based on the separated flow model.

2.2 Tube diameter for stable operation

Akachi [6] reported that the range of inner diameter for stable operation of the OCHP was 0.1 ~ 5 mm. In this range of inner diameter, the working fluid was arranged randomly into vapor plugs and liquid slugs due to the effect of surface tension. Chandratilleke et al. [10] proposed the condition of tube diameter for the generation of liquid slugs and vapor plugs inside a pipe. Rossi et al. [41] also proposed that liquid slugs and vapor plugs could exist inside a tube of 0.5 ~ 3.0 mm inner diameter for stable operation of the OCHP.

The equations for determination the inner diameter of the OCHP are the followings.

Chandratilleke's equation

$$d = (1.5 \sim 2.0)\sqrt{\frac{\sigma}{g(\rho_f - \rho_g)}} \tag{2.1}$$

Akachi & Polasek's equation

$$d \prec 2 \times \sqrt{\frac{\sigma}{\rho_f g}} \tag{2.2}$$

Nishio's Equation

$$d \prec 1.84 \times \sqrt{\frac{\sigma}{g(\rho_f - \rho_g)}} \tag{2.3}$$

Table 2.1 Inner diameters (mm) for stable operation of the OCHP

	Chandratilleke et al. $d = (1.5 \sim 2.0)\sqrt{\frac{\sigma}{g(\rho_f - \rho_g)}}$				Akachi et al. $d \prec 2 \times \sqrt{\frac{\sigma}{\rho_f g}}$				Nishio et al. $d \prec 1.84 \times \sqrt{\frac{\sigma}{g(\rho_f - \rho_g)}}$			
Temp (K)	283	303	333	353	283	303	333	353	283	303	333	353
H_2O	4.1 ~5.5	4.1 ~5.4	3.9 ~5.2	3.8 ~5.1	5.6	5.4	5.2	5.2	5.1	5.0	4.8	4.7
Ethanol	2.7 ~3.6	2.7 ~3.6	2.6 ~3.5	2.6 ~3.4	3.6	3.6	3.4	3.4	3.3	3.3	3.2	3.2
R141b	1.9 ~2.6	1.8 ~2.4	1.7 ~2.2	1.6 ~2.1	2.6	2.4	2.2	2.2	2.4	2.0	2.0	2.0
R142b	1.7 ~2.2	1.5 ~2.0	1.3 ~1.7	1.2 ~1.5	2.2	2.0	1.8	1.4	2.0	1.9	1.6	1.4

The related equations showed that the inner diameters were determined by holding the surface tension and gravitational force of working fluid in an equilibrium state to form liquid slugs and vapor plugs inside the OCHP. The working fluids with large surface tension and small fluid density gave a large range of inner diameter for forming capillary slug flow.

Table 2.1 presented the ranges of inner diameters for stable operation of the OCHP at the different temperature of some common working fluid. As shown in Table 2.1, the inner diameters for stable operation became smaller by increasing the working temperature. This was due to the fact that the surface tension and liquid density decreased as the working temperature increased. The inner diameter ranges at the same temperature condition of R142b, R141b, ethanol and water were large in turn. The inner diameter range of water showed a big difference in compare with three kinds of remaining working fluids. The reason was that the surface tension of water was much bigger than that of other working fluids.

2.3 Fundamental processes in the OCHP

Before attempting the development of numerical analysis for the operating mechanism of the OCHP, it is necessary to consider the fundamental processes, which occur in the operation of the OCHP. Figure 2.4 suggests the various forces, heat and mass transfer processes acting on a typical capillary slug flow as shown in Fig. 2.1. It is emphasized that scrutinizing the same control volume on an OCHP will, in general, manifest much more complicated molecular forces, heat and mass transfer processes than what has been depicted in Fig. 2.4. Therefore only the primary processes have been summarized below:

- Liquid slugs have menisci on the slug edges due to surface tension forces.
- A liquid thin film may exist surrounding vapor plugs.

- The contact angle of the menisci and the thickness of the liquid thin film depend on the fluid-solid combination and the operating parameters.
- Liquid slugs are subjected to pressure forces from the adjoining vapor plugs.
- Liquid slugs and vapor plugs may receive heat, reject heat or move without any external heat transfer depending on their location in the evaporating section, condensing section or adiabatic section, respectively.
- In the evaporating section, liquid slugs receive heat and simultaneously follow by evaporation mass transfer to the adjoining vapor plugs. Also, some liquid slugs are broken up due to the generation of bubbles by nucleate boiling.
- Probability of events frequently places vapor plugs in direct contact with the tube surface in the evaporating section. In this case, vapor plugs receive heat and evaporation mass transfer from the adjoining liquid slugs. Consequently, the saturation pressure and temperature locally increase in the evaporating section.
- The above processes as described for the evaporating section are repeated in a reverse direction for the condensing section.
- In the adiabatic section, while passing from the evaporating section to the condensing section, the train of vapor-liquid slug-train units are subjected to a series of complex heat and mass transfer processes. Essentially non-equilibrium conditions exist whereby the liquid and vapor plugs saturated at the high pressure and temperature are brought down to saturated conditions at the low pressure and temperature existing in the condensing section. In real systems this transit is certainly much more complex with non-equilibrium conditions existing throughout the flow channels of the OCHP.

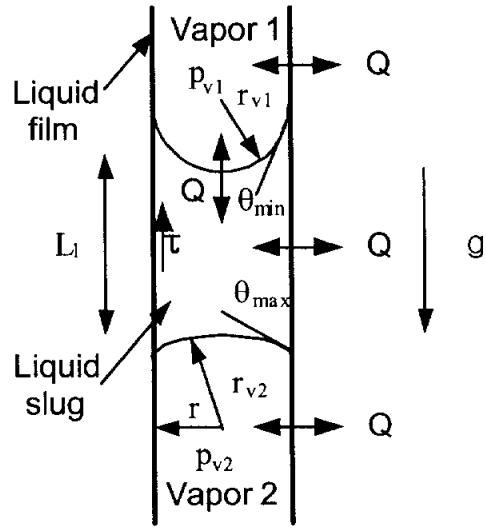

Fig. 2.4 Transport processes in an OCHP

A simple momentum equation can be solved in order to predict the length of liquid slugs. When a liquid slug is formed, gravity naturally tends to pull the liquid downward. However, as downward motion begins, the contact angles at top and bottom of the liquid slug must be receding and advancing, respectively. Force balance requires that

$$p_{v1}\pi r^2 - p_{v2}\pi r^2 + \rho_l g L_l \pi r^2 + 2\pi r_{v2}\sigma - 2\pi r_{v1}\sigma = 0 \tag{2.4}$$

Assuming that the pressure difference between the two vapor plugs has a relation as

$$p_{v2} = p_{v1} + \rho_v g L_l \tag{2.5}$$

Combining Eq. (2.5) into Eq. (2.4) results in

$$L_l = \frac{2\sigma}{r(\rho_l - \rho_v)g}\left(\frac{r_{v1} - r_{v2}}{r}\right) \tag{2.6}$$

Assuming that θ_{min} and θ_{max} have minimum and maximum value, the initial length of the liquid slugs that can be supported against gravity can be expressed in the following equation

$$L_l = \frac{2\sigma}{r(\rho_l - \rho_v)g}(\cos\theta_{min} - \cos\theta_{max}) \tag{2.7}$$

As shown in Eq. (2.7), it is obvious that physical effects, fluid properties and geometrical factors influence each other on the initial state of the OCHP.

When heat was applied to the OCHP, the processes of heat and mass transfer of liquid slugs and vapor plugs might occur as mentioned above. It was to be noted that there occurred no steady state in the operation of the OCHP. The non-equilibrium state in the operation of the OCHP can be simplified as the followings:

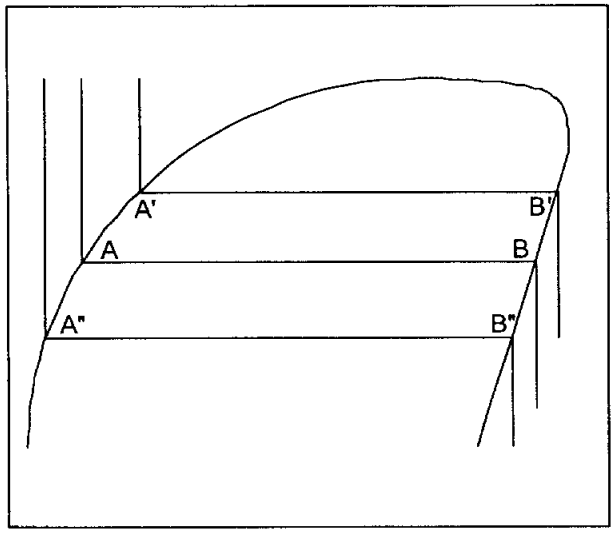

Fig. 2.5 Pressure-enthalpy diagram

Consider a case when an OCHP is kept throughout isothermal. In this case the liquid and vapor phases inside the OCHP must exist in equilibrium at the saturated pressure corresponding to the fixed isothermal temperature. Referring to the pressure-enthalpy diagram as shown in Fig. 2.5, the thermodynamic state of all liquid slugs, irrespective of their size and position, can be represented by point A. Similarly point B represents the thermodynamic state of all vapor plugs presented in the OCHP. Suppose the temperature of the entire structure of the OCHP is now quasi-statically increased to a new constant value, then the system will again come to a new equilibrium temperature and corresponding saturation pressure, point A' and B' in Fig. 2.5. In doing so, there will be some evaporation mass transfer from the liquid until equilibrium is reached again. A similar phenomenon will be observed if the OCHP is quasi-statically cooled to new equilibrium conditions, point A" and B" (exaggerated representation for clarity).

In an actual operation of the OCHP, there exists a temperature gradient between the evaporating section and condensing section. The effect of this temperature gradient in the OCHP is to cause non – equilibrium pressure condition which is the primary force for the transport of working fluid. The heating process in the evaporating section continuously tries to push the point A upwards on the liquid saturation line of the pressure – enthalpy diagram. Simultaneously the point B is forced to move downwards on the vapor line. In this way a sustained non – equilibrium state exists between the driving thermal potentials and the natural causality, which tries to equalize the pressure in the OCHP. This effect causes oscillation of liquid slugs and vapor plugs in each of the individual flow channels, which interact with each other possibly generating pressure waves in the OCHP.

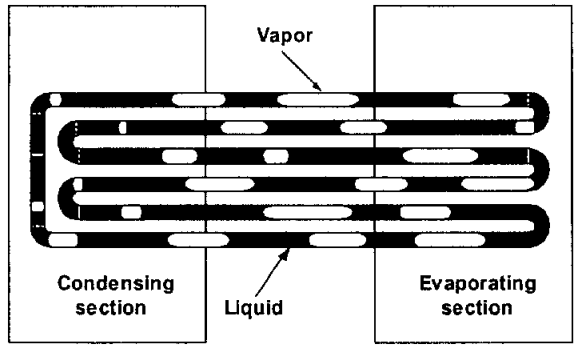

(a) Loop type OCHP

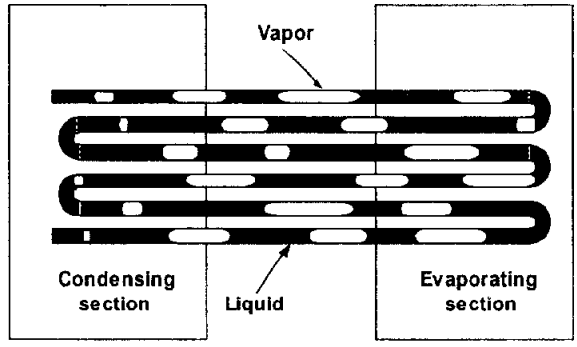

(b) Non-loop type OCHP

Fig. 2.6 Schematic of two types of the OCHP

2.4 Effect of the type of the OCHP

There are two types of the OCHP as shown in Fig. 2.6. The loop type OCHP, which has two open ends, connected to one another (Fig. 2.6(a)). The non-loop type OCHP, which has two unconnected ends (Fig. 2.6(b)).

The oscillation of liquid slugs and vapor plugs in the channels of the loop type OCHP was more active than that in the non-loop type OCHP because the two ends of the loop type were connected to each other. Also the working fluid could circulate in the entire structure of the loop type OCHP. The direction of the circulation (clockwise or anti-clockwise) for the working fluid in the loop type

was arbitrary during steady operation state. The randomness in the direction of the circulation could be attributed to the uneven distribution of liquid slugs and vapor plugs as well as their positions in the OCHP. The effect of the circulation enhanced the capability for working fluid to transport heat from the evaporating section to the condensing section in the loop type OCHP.

2.5 Effect of the turn number of the OCHP

When the turn number of the OCHP was increased, the capillary slug flow pattern in which vapor plugs and liquid slugs were well divided was represented. The flow was very active in the condensing section. Also the circulation of the working fluid in the total flow of the loop type OCHP was more active. The working fluid in the total flow circulated to one direction in the OCHP. The total flow circulated rapidly as well as forming the wave from the left side to the right side or reverse of the OCHP. This flow pattern could not be observed at the small turn number of the loop type OCHP in the same conditions. This was due to the fact that when the turn number was small the degree of the freedom of oscillation flow was small [48]. Miyazaki et al. [16] also confirmed the existence of the oscillation waveform of working fluid by flow visualization experiments using the OCHP of 25 turns. They concluded that the occurrence of the oscillation wave was due to the pressure wave within the OCHP.

Figure 2.7 depicts a rapid waveform by inter-connecting the ends of long liquid slugs at each flow channel. The frequency of the oscillation was high when the circulation and oscillation of liquid slugs and vapor plugs were most active. The frequency of the oscillation was influenced by the heat flux (to the evaporating section). It was noted that the variation of the oscillation frequency corresponded to the oscillation pressure in the evaporating section of the OCHP [48].

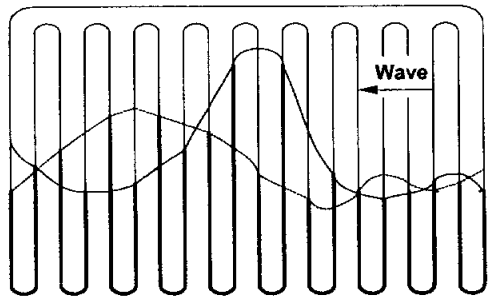

Fig. 2.7 Schematic diagram of oscillating wave in the OCHP of 10 turns

Chapter 3

Numerical analysis of the OCHP based on the homogeneous flow model

In this chapter, a homogeneous flow model of the OCHP was developed to model the oscillating motion of working fluid in the OCHP. The differential equations of two-phase flow were applied and simultaneous non-linear partial differential equations were solved. From the analysis of the numerical results, it was found that the oscillating motion of working fluid in the OCHP was affected by the operation and design conditions such as the heat flux, the charging ratio of working fluid and the hydraulic diameter of flow channel. The numerical results showed that the proposed model and solution could be used for estimating the operating mechanism in the OCHP.

3.1 Theoretical model

Figure 3.1 illustrates a schematic of the homogeneous flow model of the OCHP with two channels that is partially filled with a working fluid. As heating is applied to the evaporating section and cooling is applied to the condensing section

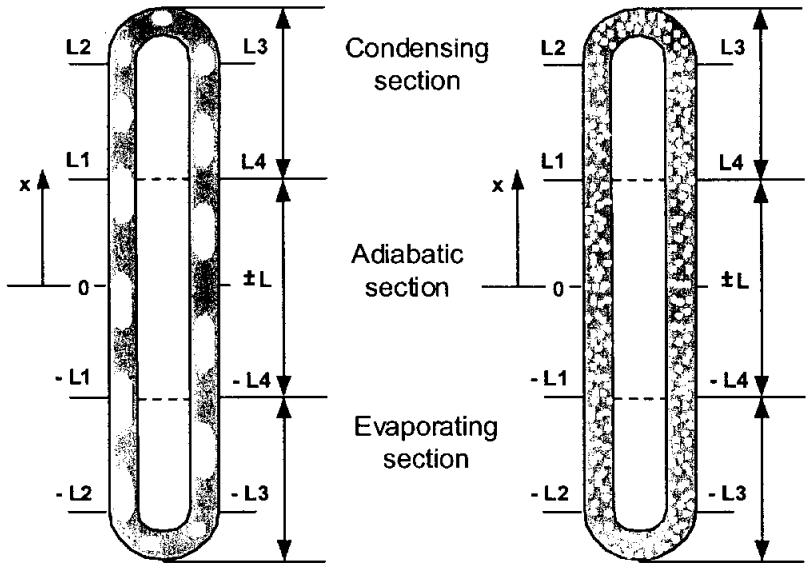

Fig. 3.1 Schematic of the homogeneous flow model of the OCHP

of the OCHP, vapor bubbles generate in the evaporating section and the condensation of vapor plugs simultaneously occurs in the condensing section. The volume expansion due to the vaporization and the contraction due to the condensation cause an oscillating motion of working fluid that propels vapor plugs (carrying heat) toward the condensing section and returns liquid to the evaporating section. The oscillatory motion of liquid slugs and vapor plugs is self-sustained as long as the heating and cooling conditions are maintained.

3.2 Derivation of governing equations

The following assumptions are made in developing the simplified form for the derivation of governing equations.

i. The phases of working fluid are in thermo-dynamic equilibrium.

ii. Flow model is homogeneous and there is a no-slip flow.

iii. Flow model is a one-dimensional model.

iv. Contribution of the kinetic and pressure energy terms in the energy equation is small compared to the enthalpy of the fluid and the heat transfer rates.

Depending on the above assumptions, the governing equations for the control volume of the OCHP can be written as follows.

- Momentum equation

Using the relation, $G = \rho V$, the momentum equation is [49]

$$\frac{\partial G}{\partial t} + \frac{\partial}{\partial x}\left(\frac{G^2}{\rho}\right) = -\frac{\partial p}{\partial x} - F \pm \rho g \tag{3.1}$$

where, the first term on the right side of Eq. (3.1) gives the total static pressure gradient as evaluated from the homogeneous flow model, the second term gives the total wall shear force per unit volume of pipe and the third term is the effect of the gravity force.

- Energy equation

The energy equation can be expressed in terms of the enthalpy and mass velocity as [49]

$$\rho\frac{\partial h}{\partial t} + G\frac{\partial h}{\partial x} = \pm\frac{4}{d}q \tag{3.2}$$

where, h is the specific enthalpy of the homogeneous flow and the right side of Eq. (3.2) represents the heat transfer rate between the pipe wall and working fluid.

3.3 Numerical procedure

Assuming that the heat inputted to the evaporating section and the heat rejected from the condensing section is constant, q_0. The heat flux, q, is expressed in the following form

$$q = f(x) = \begin{cases} q_0 \ (-L_4 \le x \le -L_1) & (Evaporating\ section) \\ 0 \ (-L_1 < x < L_1) & (Adiabatic\ section) \\ 0 \ (L_4 < x \le L) & (Adiabatic\ section) \\ 0 \ (-L \le x < -L_4) & (Adiabatic\ section) \\ -q_0 (L_1 \le x \le L_4) & (Condensing\ section) \end{cases} \tag{3.3}$$

Approximating the above Eq. (3.3) to the Fourier series on displacement [-L ~ L] [49]

$$f(x) = \frac{a_0}{2} + \sum_{n=1}^{\infty} \left[a_n \cos\left(\frac{n\pi x}{L}\right) + b_n \sin\left(\frac{n\pi x}{L}\right) \right] \tag{3.4}$$

where a_n, b_n, are the Fourier series coefficients. Because $f(x)$ is "odd function", Eq. (3.4) can be expressed in the form of Fourier cosines series as follow [50]

$$f(x) = \sum_{n=1}^{\infty} \left[\frac{2q_o}{\pi n} \left(\cos\frac{n\pi L_4}{L} - \cos\frac{n\pi L_1}{L} \right) \times \sin\left(\frac{n\pi x}{L}\right) \right] \tag{3.5}$$

Approximate heat flux function, Eq. (3.5), is plotted with different values of n as shown in Fig. 3.2. At $n = 100$, it is found that heat flux q is approximated to a constant value of q_0 at the evaporating section and condensing section.

The frictional force per unit volume of pipe F can be expressed in terms of a two-phase friction factor f as follows [49]

$$F = \frac{4}{d}\tau_w = \frac{4}{d}\left[f\left(\frac{\rho V^2}{2}\right) \right] = \frac{2}{\rho d} G^2 f \tag{3.6}$$

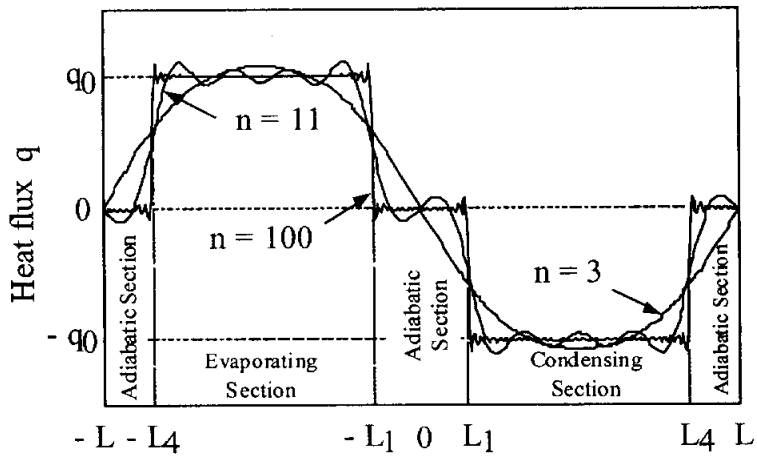

Fig. 3.2 Approximation of heat flux distribution

Subject to assumption (ii) above, using the homogeneous model it is necessary to apply suitably defined single-phase friction factor to two-phase flow. The two-phase friction factor f has been evaluated using a mean two-phase viscosity μ in the normal friction factor relationships with assuming that the friction factor may be expressed in terms of the Reynolds number by the Blasius equation [51].

$$f = 0.079\left(\frac{Gd}{\mu}\right)^{-1/4} \tag{3.7}$$

where, $$\frac{1}{\mu} = \frac{X}{\mu_g} + \frac{1-X}{\mu_f} \tag{3.8}$$

The pressure gradient is proportional to mass flow rate, $\dot{m}$, was introduced by Miyazaki et al. [28] as follows

$$-\frac{\partial p}{\partial x} = \dot{m}\frac{128\upsilon}{\pi d^4} = \frac{32\upsilon}{d^2}G \tag{3.9}$$

The homogeneous flow density ρ, specific volume v and specific enthalpy h can be expressed in the quality X of mixed flow as follows.

$$\rho = \rho_f + X(\rho_g - \rho_f) = \rho_f + X\rho_{fg} \tag{3.10}$$

$$v = v_f + X(v_g - v_f) = v_f + Xv_{fg} \tag{3.11}$$

$$h = h_f + X(h_g - h_f) = h_f + Xh_{fg} \tag{3.12}$$

Substituting Eqs. (3.3) ~ (3.12) into Eqs. (3.1) ~ (3.2), and rearranging, the momentum and energy equations are changed to the following general equations.

$$\frac{\partial G}{\partial t} + G^2 v_{fg}\frac{\partial X}{\partial x} = \frac{32\upsilon}{d^2}G - \frac{2}{\rho d}G^2 f - (\rho_f + X\rho_{fg})g \tag{3.13}$$

$$\frac{\partial X}{\partial t} + (v_f + Xv_{fg})G\frac{\partial X}{\partial x} = -(v_f + Xv_{fg})\frac{8q_0}{dh_{fg}} \times \sum_{n=1}^{100}\left[\frac{1}{\pi n}\left(\cos\frac{n\pi L_4}{L} - \cos\frac{n\pi L_1}{L}\right)\sin\frac{n\pi x}{L}\right] \tag{3.14}$$

where the vapor quality, X, is correlated with the charging ratio, α , through the model proposed by Abdul-Razzak [52]. It can be expressed in the following form using the Martinelli parameter, X_{tt}

$$\alpha = \frac{1}{1 + 0.49X_{tt}^{0.803}} \tag{3.15}$$

where

$$X_{tt} = \left(\frac{1-X}{X}\right)^{0.9}\left(\frac{\rho_g}{\rho_f}\right)^{0.5}\left(\frac{\mu_f}{\mu_g}\right)^{0.1} \tag{3.16}$$

The equations (3.13) and (3.14) are nonlinear partial differential equations, which decide the variations of G and X . The numerical analysis is conducted by using method introduced by Maezawa et al. [33] as follows.

The general solution of the quality, $X(x,t)$, is approximate using a Fourier series as follows.

$$X(x,t) = X_0 + \sum_{n=1}^{\infty}\left[X_1(t)\cos\left(\frac{n\pi x}{L}\right) + X_2(t)\sin\left(\frac{n\pi x}{L}\right)\right] \tag{3.17}$$

where $X_1(t)$ and $X_2(t)$ are the Fourier coefficients which are the time dependent variables.

For n = 1, Eq. (3.17) becomes

$$X(x,t) = X_0 + X_1(t)\cos\left(\frac{\pi x}{L}\right) + X_2(t)\sin\left(\frac{\pi x}{L}\right) \tag{3.18}$$

Substituting Eq. (3.18) into the momentum equation (3.13) and energy equation (3.14) and considering the mass velocity G is constant along the closed loop of the OCHP [33]. Eqs. (3.13) and (3.14) changed to the following equations.

$$\frac{dG}{dt} = \frac{32\upsilon}{d^2}G - \frac{2v_f}{d}G^2 f - \left(\frac{2v_{fg}}{d}G^2 f + \rho_{fg} g\right)\left(X_0 + X_1\cos\frac{\pi x}{L} + X_2\sin\frac{\pi x}{L}\right) - \rho_f g \tag{3.19}$$

$$\left(\frac{dX_1}{dt} + X_2\frac{G\pi}{\rho_0 L}\right)\cos\frac{\pi x}{L} +$$

$$\left(\frac{dX_2}{dt} - X_1\frac{G\pi}{\rho_0 L} - \frac{8q_0}{\rho_0 d h_{fg}\sin(\pi x/L)}\sum_{n=1}^{100}\left[\frac{1}{\pi n}\left(\cos\frac{n\pi L_4}{L} - \cos\frac{n\pi L_1}{L}\right)\right]\right)\sin\frac{\pi x}{L} = 0 \tag{3.20}$$

From Eqs. (3.19) and (3.20) we can find out new equations according to the coefficients of each harmonics as the following ordinary differential equations.

$$\frac{dG}{dt} = \frac{32\upsilon}{d^2}G - \frac{2v_f}{d}G^2 f - \left(\frac{2v_{fg}}{d}G^2 f + \rho_{fg} g\right)\left(X_0 + X_1\cos\frac{\pi x}{L} + X_2\sin\frac{\pi x}{L}\right) - \rho_f g \tag{3.21}$$

$$\left(\frac{dX_1}{dt} + X_2\frac{G\pi}{\rho_0 L}\right) = 0 \tag{3.22}$$

$$\left(\frac{dX_2}{dt} - X_1\frac{G\pi}{\rho_0 L} - \frac{8q_0}{\rho_0 dh_{fg}\sin(\pi x/L)}\sum_{n=1}^{100}\left[\frac{1}{\pi n}\left(\cos\frac{n\pi L_4}{L} - \cos\frac{n\pi L_1}{L}\right)\right]\right) = 0 \qquad (3.23)$$

It is evident that these three equations are non-linear ordinary differential equations, which decide the temporal change of G, X_1, and X_2 totally. When using high order harmonic (for n > 1), we can find out the same ordinary equations [33]. There was not contribution of the non-linear term $G^2 v_{fg}\frac{\partial X}{\partial x}$ in the left side of the momentum equation because it can be cut off based on the function form of x [33].

The system of ordinary differential equations (3.21) ~ (3.23) are solved using Runge-Kutta fourth order method.

Initial conditions: $X = X_0, \quad X_1 = X_2 = 0, \quad t = 0, \qquad (3.24)$

$G = 0, \quad t = 0 \qquad (3.25)$

Boundary conditions: because the model is a loop type OCHP, the boundary conditions can be ignored due to the connection of the ends together.

For conducting numerical analysis, R-142b is chosen as the working fluid. The parameters used in the numerical modeling are listed in Table 3.1

Table 3.1 Modeling parameters.

Parameters	Values	Parameters	Values
d [mm]	1.5, 3	α_0 [vol.%]	20, 40, 80
ρ_f [kg/m^3]	1097	ρ_g [kg/m^3]	17.721
v_f [m^3/kg]	0.912e-3	v_g [m^3/kg]	56.43e-3
h_f [J/kg]	233280	h_g [J/kg]	429960
υ_f [m^2/s]	0.256e-6	υ_g [m^2/s]	0.603e-6
L [m]	0.220	q_o [W/cm^2]	0.5, 1, 2

3.4 Numerical results

At the heat flux condition of 1 W/cm^2, the variations of the numerical mass velocity G with respect to time according to the different charging ratios of working fluid are shown in Fig. 3.3. The oscillation of the mass velocity G was almost symmetric at the charging ratio of 80 vol.% as shown in Fig. 3.3(a). However, the oscillation of the mass velocity was unsteady due to the increase of oscillation amplitude and the decrease of frequency. The flow visualization experiments also confirmed that the operating state of the OCHP changed to an unsteady state at the charging ratio of 80 vol.% [26, 27].

Figure 3.3(b) shows the oscillation of the mass velocity G at the charging ratio of 40 vol.%. The oscillation of the mass velocity was steady. The charging ratio of 40 vol.% could be expected as the optimal charging ratio of the OCHP predicted by theoretical model. The active oscillations of working fluid were also observed at the charging ratio of 40 vol.% through the flow visualization experiments [14, 15].

Figure 3.3(c) shows the oscillation of the mass velocity G at the charging ratio of 20 vol.%. The oscillation was unsteady due to the decrease of oscillation amplitude. The flow visualization experiments showed that the oscillation phenomenon in the OCHP was low and unsteady at this charging ratio due to the lack of the liquid in the OCHP [26, 27].

When the charging ratio of working fluid was 40 vol.%, the variations of the numerical mass velocity G with respect to time according to the different heat fluxes are shown in Fig. 3.4. Figure 3.4(a) shows the oscillation of the mass velocity G at the heat flux of 0.5 W/cm^2. The oscillation of the mass velocity was unsteady due to the decrease of oscillation amplitude. This phenomenon was observed through the flow visualization experiments and was explained as follows: At the heat flux of 0.5 W/cm^2, the generation and the growth of bubbles

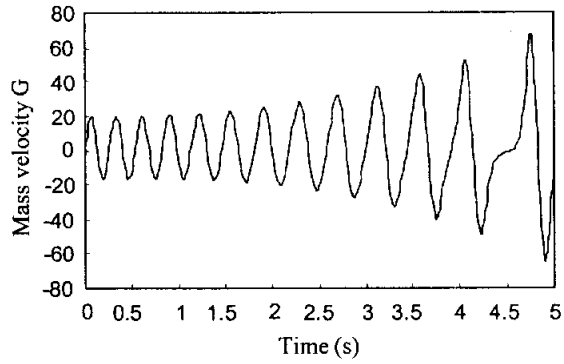

(a) α = 80 (vol. %), q = 1 (W/cm^2)

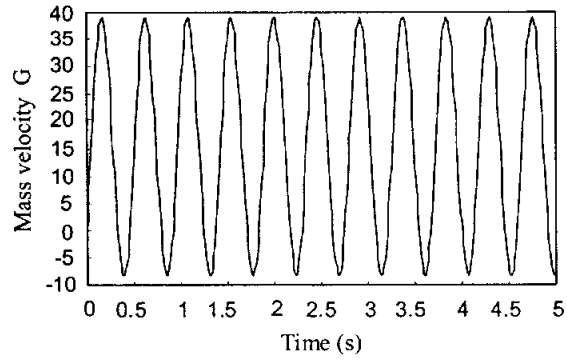

(b) α = 40 (vol. %), q = 1 (W/cm^2)

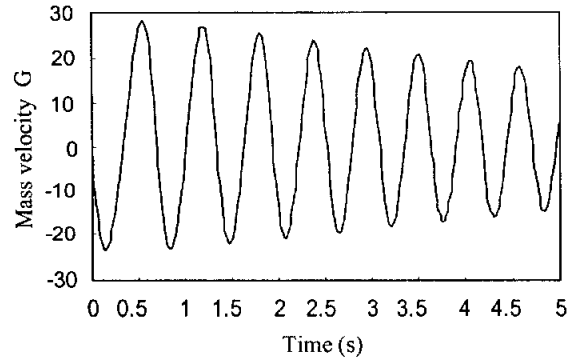

(c) α = 20 (vol. %), q = 1 (W/cm^2)

Fig. 3.3 Mass velocity according to the different charging ratios of working fluid.

in the OCHP were a nucleate boiling process at some turns among total flow channels. The bubbles grew and coalesced to become vapor plugs, and the oscillation phenomenon in that turns occurred. At the remaining turns of total flow channels, bubbles were intermittently generated, and the oscillation phenomenon was not clearly confirmed. Because of the inter-connection of the channels, the oscillation of the mass velocity in the total flow channels decreased.

When the heat flux was increased to more than 1 W/cm^2, the oscillation of vapor plugs and liquid slugs occurred very actively in each flow channel. The steady state operation of the OCHP was obtained when the heat flux was continuously increased. The numerical prediction of the mass velocity presented in Fig. 3.4(b) shows that the oscillation of the mass velocity was also steady at the heat flux condition of 1.2 W/cm^2.

When the heat flux was increased to 1.5 W/cm^2, the oscillation amplitude reduced as shown in Fig. 3.4(c). This was due to the fact that the local dry-out phenomenon occurred at some channels in the evaporating section. Because of the interconnection of the channels in the OCHP, the oscillation of vapor plugs and liquid slugs in the total flow channels gradually decreased. Consequently, the oscillation of the mass velocity in the OCHP decreased.

However, as the heat flux was continuously increased, the working fluid supplied to the evaporating section was not sufficient. The dry-out phenomena occurred in many flow channels of the OCHP and the oscillation of vapor plugs and liquid slugs became slow. Some of the flow channels in the evaporating section started to be filled with vapor phase. The supply of working fluid to the evaporating section reduced. This led to an increase in the surface temperature of the channels in the evaporating section. The liquid condensed in the condensing section was evaporated at the superheated tube wall before arriving normally in the evaporating section. Only the vapor phase existed in the evaporating section.

Hence, the oscillation phenomenon gradually reduced and finally stopped. As shown in Fig. 3.4(d), the mass velocity G reduced to zero when the heat flux was increased to q = 2 W/cm^2.

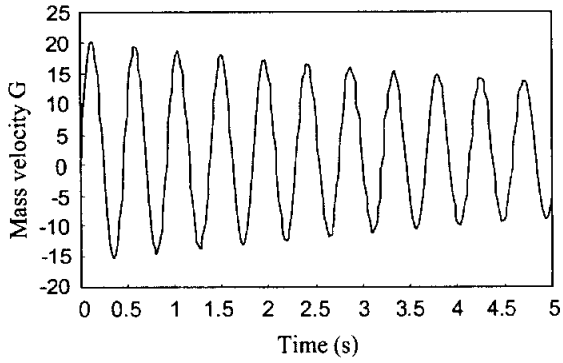

(a) q = 0.5 (W/cm^2), α = 40 (vol.%)

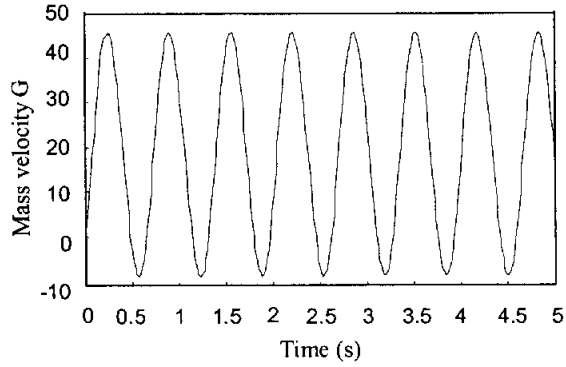

(b) q = 1.2 (W/cm^2), α = 40 (vol.%)

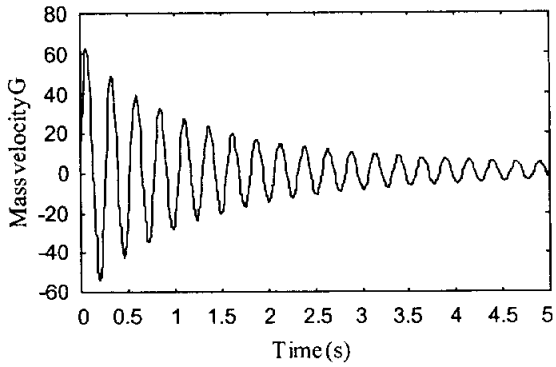

(c) q = 1.5 (W/cm^2), α = 40 (vol.%)

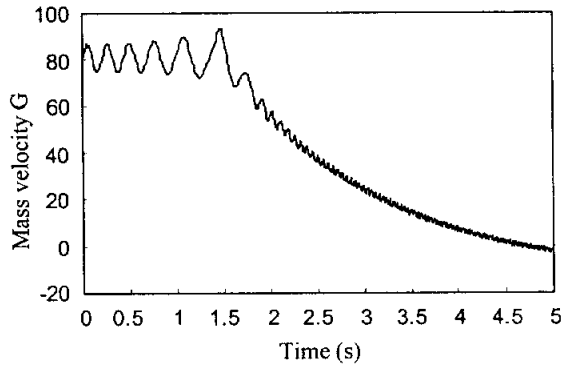

(d) q = 2 (W/cm^2), α = 40 (vol.%)

Fig. 3.4 Mass velocity according to the different heat fluxes

The oscillating motion of working fluid in the OCHP was also affected by the cross section geometry of the flow channel. When the charging ratio of working fluid was 40 vol.% and the heat flux was 1 W/cm^2, the variations of the numerical mass velocity G with respect to time according to the different hydraulic diameters are shown in Fig. 3.5. In the case of 1.5 mm diameter, the oscillation was steady. When the diameter was increased to d = 3 mm, the oscillation amplitude decreased. From flow visualization experiments, it could be explained that the surface tension force was not dominant over the gravitation force in a

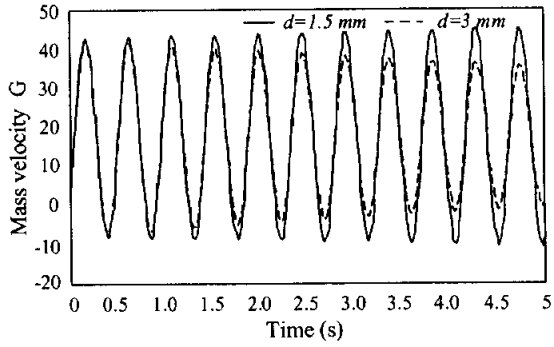

Fig. 3.5 Mass velocity according to the different hydraulic diameters

large diameter tube. Furthermore, during the initial period, at the moment after working fluid was partially filled in the OCHP, the generation of vapor-liquid slug-train units by capillary force reduced in the large diameter tube. Consequently, the oscillation of working fluid decreased when heat was applied to the evaporating section of the OCHP.

3.5 Comparisons with previous experimental results

It is necessary to compare the numerical results with the experimental results reported in the literature. Due to the limited availability of data for the OCHP with the same conditions of the parameters covered in the present study, the comparisons are only possible for a few cases.

Figure 3.6 illustrates the influence of heat flux and charging ratio on the effective thermal conductivity obtained by Lee [27]. The effective thermal conductivity was maximal at the charging ratio of 40 vol.% and the heat flux of 1 W/cm^2. This was due to the fact that the oscillation of working fluid occurred actively in each flow channel in the OCHP. The pressure wave was a sinusoidal waveform, the pressure difference (between the evaporating section and the

condensing section) was at the least, the oscillation amplitude of pressure wave was at the least, and the frequency of pressure oscillation was the highest [27]. As shown in Fig. 3.3(b), the oscillation of the mass velocity got steady state at the same conditions of the heat flux and charging ratio as mentioned above. The charging ratio of 40 vol.% and the heat flux of 1 W/cm^2 were expected as the optimal operation conditions of the OCHP predicted by theoretical model. It could be concluded that there was an agreement between the experimental results and the numerical results at the heat flux of 1 W/cm^2 and the charging ratio of 40 vol.%.

When the charging ratio was 40 vol.%, the experimental results of the surface temperature at some locations of the OCHP with heat flux is shown in Fig. 3.7. At the heat fluxes below 1.25 W/cm^2, the surface temperatures in the evaporating section and condensing section were almost similar, and the steady state operation of the OCHP was obtained. When the heat flux was increased to 1.25 W/cm^2, the surface temperature in the evaporating section suddenly increased from the leading edge. As the heat flux continuously increased to more than 1.5 W/cm^2, the surface temperature in many locations of the evaporating section increased. The oscillation of working fluid in the OCHP changed to an unsteady-state due to dry-out phenomena occurring in the evaporating section of the OCHP. The surface temperature of the channels in the evaporating section increased. Hence the heat transfer rate decreased. As shown in Figs 3.4(c) and 3.4(d), the local dry-out phenomena started to occur when the heat flux increased to 1.5 W/cm^2 by theoretical model. Also the numerical results showed that the mass velocity in the OCHP reduced to zero when the dry-out phenomena occurred in the total flow channels of the OCHP. The heat flux of 2 W/cm^2 was expected as the operation limit of the OCHP due to the dry-out phenomena. In comparison with the experimental results as shown in Fig. 3.7, one can conclude that the theoretical model was also well predicted for a situation where the dry-out phenomena

occurred in the OCHP.

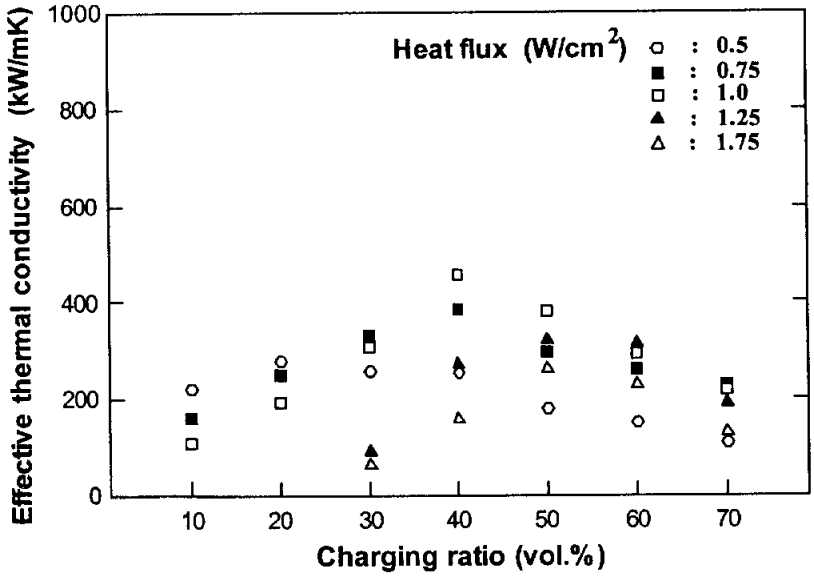

Fig. 3.6 Effective thermal conductivity with heat flux and charging ratio [27].

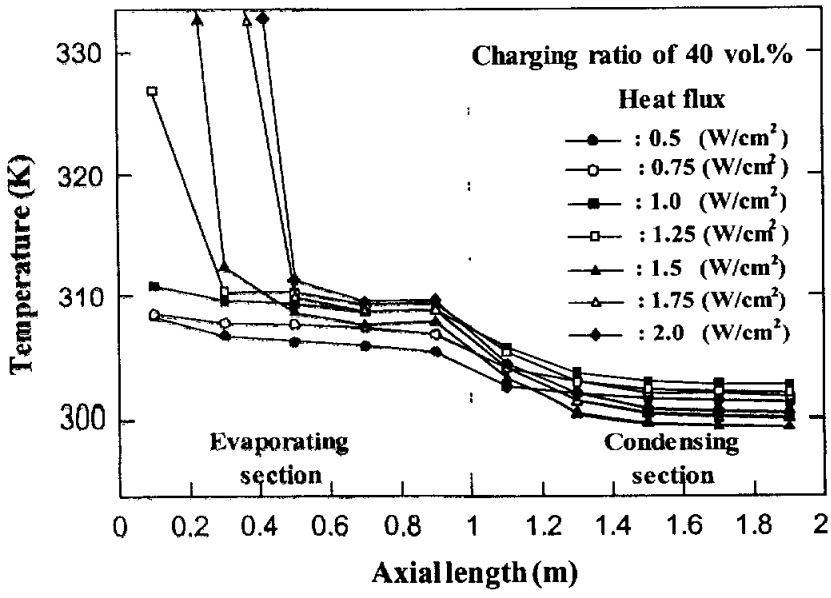

Fig. 3.7 Surface temperature at some locations of the OCHP with heat flux [27].

Figure 3.8 shows the pressure obtained in the theoretical model at the heat flux of 1.2 W/cm^2. The numerical pressure was calculated by using Eq. (3.9). Comparison with the experimental pressure data at the same heat flux condition obtained by Jung [53] is also shown in Fig. 3.8. These experimental pressure data were measured at a flow channel in the evaporating section of the OCHP. The experimental pressure data matched the numerical results well as shown in Fig. 3.8. There was only an error around 5% in comparison of the average values between the experimental pressure and the numerical pressure. This implied that the homogeneous flow model could be used to model the flow of working fluid in the evaporating section of the OCHP.

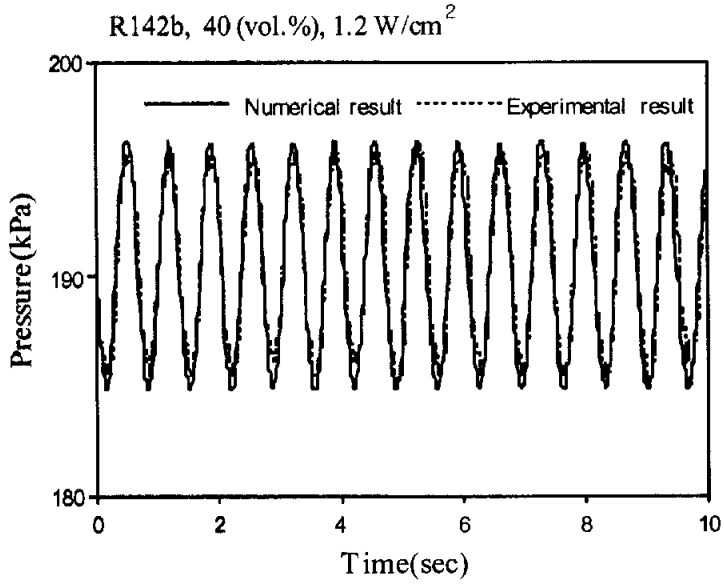

Fig. 3.8 Comparison between numerical and experimental pressure data [53].

3.6 Summary

A theoretical model of the OCHP was developed to model the oscillating motion of working fluid in the OCHP. The mass velocity in the OCHP was solved based on the theoretical model and the differential equations of two-phase flows in the OCHP. The following conclusions were obtained.

- The oscillation of the mass velocity was steady at the charging ratio of 40 vol.%. The charging ratio of 40 vol.% was predicted as the optimal charging ratio in the operation of the OCHP.
- The dry-out phenomena occurred when the heat flux was increased to 1.5 W/cm^2 at the charging ratio of 40 vol.%.
- The heat flux of 2 W/cm^2 was confirmed as the operation limit of the OCHP due to the dry-out phenomena at the charging ratio of 40 vol.%.
- There was an agreement between the numerical pressure and the experimental pressure data at the heat flux of 1.2 W/cm^2, the charging ratio of 40 vol.%, and the working fluid of R-142b.
- When the hydraulic diameter of the OCHP was increased to 3 mm, the oscillation amplitude of the mass velocity decreased.

Chapter 4

Numerical analysis of the OCHP based on the separated flow model

Analytical model of the OCHP with two liquid slugs and three vapor plugs was presented in this chapter. The governing equations were solved using an explicit finite difference scheme to predict the behavior of vapor plugs and liquid slugs. The results showed that the diameter, surface tension, and charge ratio of working fluid have significant effects on the performance of the OCHP.

4.1 Theoretical model

Figure 4.1(a) shows a theoretical model of the OCHP. The bends are not considered and it is assumed that the OCHP is a straight tube (Fig. 4.1(b)). There are three vapor plugs and two liquid slugs in the OCHP. The pressure and the temperature of all vapor plugs are initially equal. A control volume of a liquid slug bounded with two vapor plugs is shown in Fig. 4.2. Suppose the initial value of $\Delta p = p_{vi} - p_{v(i+1)}$ is greater than zero, and part of the vapor plug in the left side of the liquid slug is in contact with the cooling section, condensation occurring in the left vapor plug will result in a decrease in the pressure of the left

vapor plug, p_{vi}. On the other hand, part of the right heating section is in contact with the liquid slug and boiling may occur at the contact area of the right heating section and liquid slug, which causes increasing the vapor pressure of the right vapor plug, $p_{v(i+1)}$. The liquid plug will be pushed back to the left side due to the pressure difference between the two vapor plugs, $\Delta p = p_{vi} - p_{v(i+1)} \prec 0$. When $\Delta p = p_{vi} - p_{v(i+1)}$ becomes zero, there is no evaporation or condensation in the two vapor plugs, but the liquid slug keeps moving due to its inertia. When part of the liquid slug enters the left heating section, part of the right vapor plug will be in contact with the cooling section. At this point, the boiling in the left vapor plug and condensation in the right vapor plug will change the sign of Δp, and this will result in the motion of the liquid slug to the right side. The oscillation of the liquid slug can be maintained by alternative evaporation or condensation in the two vapor plugs.

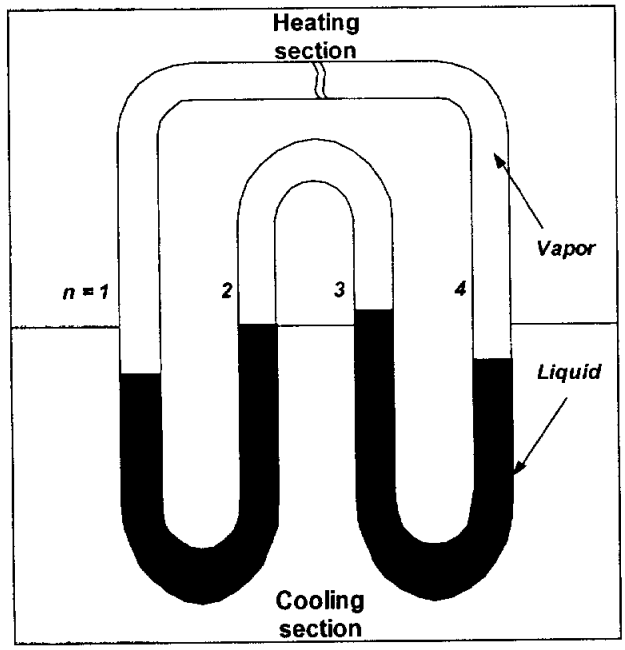

(a)

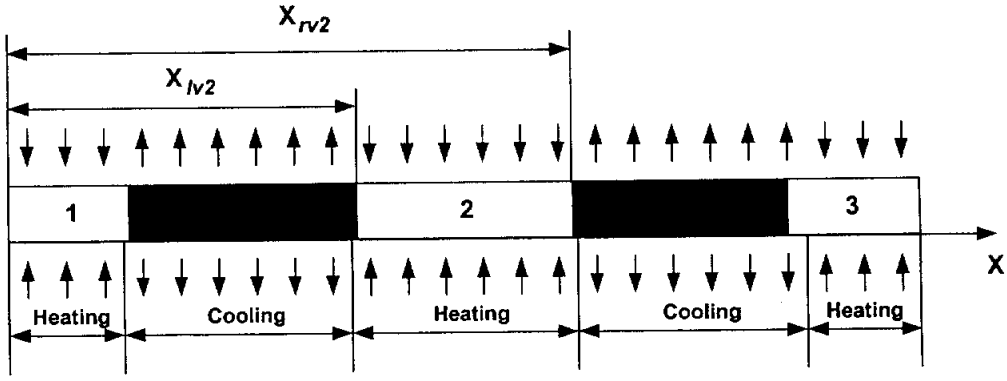

(b)

Fig. 4.1 Theoretical model of the OCHP

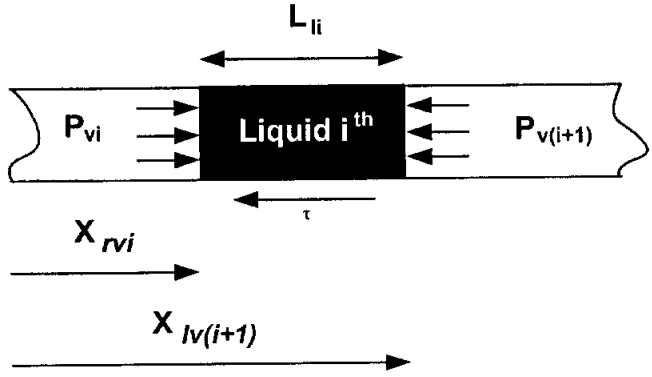

Fig. 4.2 Control volume of i^{th} liquid slug

The following assumptions are made in order to model the heat transfer and oscillation characteristics in the OCHP:

i. The liquid is incompressible and the vapor is assumed to behave as ideal gases

ii. Evaporative and condensation heat transfer coefficients are assumed to be constants

iii. Heat transport in the thin film is due only to the conduction in the radial direction

iv. The pressure losses at the bends are not considered

4.2 Derivation of governing equations

The governing equations constituting the theoretical model are derived by considering the conservation of mass, momentum and energy as applied to the vapor plugs and liquid slugs.

4.2.1 Governing equations of vapor plugs

The continuity equation for the i^{th} vapor plug is

$$\frac{dm_{vi}}{dt} = \dot{m}_{in,vi} - \dot{m}_{out,vi} \tag{4.1}$$

where $\dot{m}_{in,vi}$ is the mass flow rate transfers into the vapor plug due to evaporation, and $\dot{m}_{out,vi}$ is the mass flow rate transfers from the vapor plug due to condensation of the i^{th} vapor plug and can be calculated by the following equations:

$$\dot{m}_{in,vi} = \frac{Q_{evp,vi}}{h_{fg}} \tag{4.2a}$$

$$\dot{m}_{out,vi} = \frac{Q_{cond,vi}}{h_{fg}} \tag{4.2b}$$

where $Q_{evp,vi}$ and $Q_{cond,vi}$ represent heat transfer resulting from the evaporation and condensation of the i^{th} vapor plug

$$Q_{evp,vi} = h_{evp}\pi d L_{hi}\left(T_h - T_{vi}\right) \tag{4.3a}$$

$$Q_{cond,vi} = h_{cond}\pi d L_{ci}\left(T_{vi} - T_c\right) \tag{4.3b}$$

where h_{evp} and h_{cond} represent evaporative and condensation heat transfer coefficient, L_{hi} and L_{ci} are the length of i^{th} vapor plug in the heating and cooling section, respectively.

The energy equation for a vapor plug is

$$\frac{d(m_{vi}u_{vi})}{dt} = \dot{m}_{in,vi}h_{vi} - \dot{m}_{out,vi}h_{vi} - p_{vi}\frac{dV_{vi}}{dt} \tag{4.4}$$

Letting $u = c_vT$ and $h = c_pT$, Eq. (4.4) may be rewritten as

$$m_{vi}c_v\frac{dT_{vi}}{dt} + c_vT_{vi}\frac{dm_{vi}}{dt} = \left(\dot{m}_{in,vi} - \dot{m}_{out,vi}\right)c_pT_{vi} - p_{vi}\frac{dV_{vi}}{dt} \tag{4.5}$$

Substituting Eq. (4.1) into Eq. (4.5)

$$m_{vi}c_v\frac{dT_{vi}}{dt} = \left(\dot{m}_{in,vi} - \dot{m}_{out,vi}\right)RT_{vi} - p_{vi}A\frac{dx_{vi}}{dt} \tag{4.6}$$

The pressure of the i^{th} vapor plug, p_{vi}, is calculated by using the ideal gas law

$$p_{vi}V_{vi} = m_{vi}RT_{vi} \tag{4.7}$$

4.2.2 Governing equations of liquid slugs

The continuity equation for i^{th} liquid slug bounded with two vapor plugs as shown in Fig. 4.2 can be found from the following equation:

$$\frac{dm_{li}}{dt} = \dot{m}_{in,li} - \dot{m}_{out,li} = \frac{1}{2}\left(\frac{dm_{vi}}{dt} + \frac{dm_{v(i+1)}}{dt}\right) \tag{4.8}$$

This means that the change in mass of i^{th} liquid slug is equal to the average changes in mass of its adjacent vapor plugs.

The momentum equation for i^{th} liquid slug is

$$\frac{dm_{li}V_{li}}{dt} = \left(p_{vi} - p_{v(i+1)}\right)A - \pi dL_{li}\tau - (-1)^n m_{li}g \tag{4.9}$$

where n indicates the tube number. Since it is assumed that the OCHP is a straight tube, gravity has different signs at different locations. In the model, there are four parallel tubes, which are labeled from one to four (Fig 4.1(a)). Gravity vector is in positive direction when a liquid slug is in the first or third tubes and the gravity term in Eq. (4.9) is positive. In the second or fourth tubes the gravity vector is in the opposite direction and the gravity force term in Eq. (4.9) is negative.

The shear stress acting between i^{th} liquid slug and the tube wall can be determined from [54]

$$\tau = \frac{1}{2} f_{li} \rho_l V_{li}^2 \tag{4.10}$$

where the friction coefficient can be determined by [54] from the Hagen-Poiseuille flow

$$f_{li} = \frac{16}{\mathrm{Re}_{li}} \tag{4.11}$$

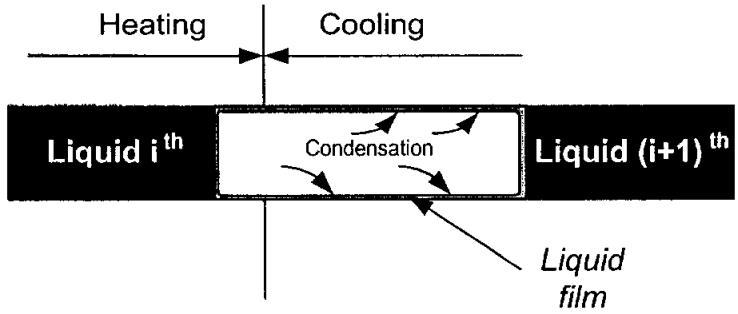

Fig. 4.3 Control volume of i^{th} vapor plug

4.2.3 Evaporation

The experimental results by flow visualization of the OCHPs in the works of Kim et al. [14, 15, 26] reveal that the generation of bubbles in the evaporating section was a nucleate boiling process. The heat transfer rate in nucleate boiling is very high, but an adequate physical description of the thermo-dynamical process is still not available. Alejandro Clausse [55] proposed a general expression to correlate the nucleate boiling regime as the following:

$$q = C(p, fluid, surface)(T_w - T_{sat})^n \tag{4.12}$$

The recommended value for the exponent n is 3.

4.2.4 Condensation

The theoretical model of film condensation in the cooling section is shown in Fig. 4.3. Because every vapor plug is bounded by two liquid slugs, the vapor velocity in the model is low in most parts of the cooling section. Also the heat transfer in the thin liquid film is assumed due only to the conduction in the radial direction. Hence, the mean value of condensation heat transfer coefficient, h_{cond}, may be determined by the following expression [51]

$$h_{cond} = 0.943\left[\frac{\rho_f(\rho_f - \rho_g)g\sin\theta h_{fg}k_f^3}{\mu_f L_c(T_{vi} - T_w)}\right]^{1/4} \tag{4.13}$$

where θ is the inclined angle of the OCHP.

4.2.5 Heat Transfer

Heat transfer in the OCHP is defined as the total heat transferred from the heating sections to the cooling sections due to evaporation and condensation of working fluid.

Evaporation and condensation heat transfer for each vapor plug can be calculated by

$$Q_{in,vi} = \dot{m}_{in,vi} h_{fg} \tag{4.14a}$$

$$Q_{out,vi} = \dot{m}_{out,vi} h_{fg} \tag{4.14b}$$

The total heat transferred into and out of the OCHP can be calculated by

$$Q_{total,in} = \sum_{i=1}^{N} Q_{in,vi} \tag{4.15a}$$

$$Q_{total,out} = \sum_{i=1}^{N} Q_{out,vi} \tag{4.15b}$$

4.3 Numerical procedure

The governing equations of vapor plugs and liquid slugs can be solved numerically by using explicit finite difference method [56]. Let m_{vi}^{new}, T_{vi}^{new}, Δx_{vi}^{new}, m_{li}^{new} and V_{li}^{new} denote the values of m_{vi}, T_{vi}, Δx_{vi}, m_{li} and V_{li} at the end of a time step. Then the finite difference equations corresponding to the governing equations are

$$\frac{m_{vi}^{new} - m_{vi}}{\Delta t} = \dot{m}_{in,vi} - \dot{m}_{out,vi} \tag{4.16}$$

$$m_{vi} c_v \frac{T_{vi}^{new} - T_{vi}}{\Delta t} = \left(\dot{m}_{in,vi} - \dot{m}_{out,vi}\right) R T_{vi} - p_{vi} A \left(\frac{\Delta x_{vi}^{new} - \Delta x_{vi}}{\Delta t} \right) \tag{4.17}$$

$$\frac{m_{li}^{new} - m_{li}}{\Delta t} = \frac{1}{2}\left[\left(\dot{m}_{in,vi} - \dot{m}_{out,vi}\right) + \left(\dot{m}_{in,v(i+1)} - \dot{m}_{out,v(i+1)}\right)\right] \tag{4.18}$$

$$\frac{m_{li}^{new}V_{li}^{new} - m_{li}V_{li}}{\Delta t} = \left(P_{vi} - P_{v(i+1)}\right)A - \pi d L_{li}\tau - (-1)^n m_{li}g \tag{4.19}$$

The values at the end of a time step can be found explicitly by using the following equations:

$$m_{vi}^{new} = m_{vi} + \left(\dot{m}_{in,vi} - \dot{m}_{out,vi}\right)\Delta t \tag{4.20}$$

$$T_{vi}^{new} = T_{vi} + \frac{\left(\dot{m}_{in,vi} - \dot{m}_{out,vi}\right)RT_{vi}\Delta t - p_{vi}A\left(\Delta x_{vi}^{new} - \Delta x_{vi}\right)}{m_{vi}c_v} \tag{4.21}$$

$$p_{vi}^{new} = \frac{m_{vi}^{new}RT_{vi}^{new}}{V_{vi}} \tag{4.22}$$

$$m_{li}^{new} = m_{li} + \frac{1}{2}\left[\left(\dot{m}_{in,vi} - \dot{m}_{out,vi}\right) + \left(\dot{m}_{in,v(i+1)} - \dot{m}_{out,v(i+1)}\right)\right]\Delta t \tag{4.23}$$

$$m_{l1}^{new} = m_{l1} + \left[\left(\dot{m}_{in,v1} - \dot{m}_{out,v1}\right) + \frac{1}{2}\left(\dot{m}_{in,v2} - \dot{m}_{out,v2}\right)\right]\Delta t \tag{4.23a}$$

$$m_{l(N-1)}^{new} = m_{l(N-1)} + \left[\frac{1}{2}\left(\dot{m}_{in,v(N-1)} - \dot{m}_{out,v(N-1)}\right) + \left(\dot{m}_{in,vN} - \dot{m}_{out,vN}\right)\right]\Delta t \tag{4.23b}$$

$$m_{li}^{new}V_{li}^{new} = m_{li}V_{li} + \left[\left(P_{vi} - P_{v(i+1)}\right)A - \pi d L_{li}\tau - (-1)^n m_{li}g\right]\Delta t \tag{4.24}$$

The displacement and the end positions of the vapor plugs at each time step can be found by using the liquid slug velocity obtained from Eq. (4.24) as follows

$$\begin{cases} x_{rv,i}^{new} = x_{rv,i} + V_{li}\Delta t \\ x_{lv,i}^{new} = x_{lv,i} + V_{l(i-1)}\Delta t \end{cases} \tag{4.25}$$

$$\begin{cases} x_{rv,N} = L \\ x_{lv,1} = 0 \end{cases} \tag{4.26}$$

where N is the number of vapor plugs, $x_{lv,i}$ and $x_{rv,i}$ are the left and right coordinates of i^{th} vapor plug measured from the origin as shown in Fig. 4.1(b)

$$\begin{cases} \Delta x_{rv,i}^{new} = x_{rv,i}^{new} - x_{rv,i} \\ \Delta x_{lv,i}^{new} = x_{lv,i}^{new} - x_{lv,i} \end{cases} \tag{4.27}$$

$$\begin{cases} \Delta x_{rv,N}^{new} = 0 \\ \Delta x_{lv,1}^{new} = 0 \end{cases} \tag{4.28}$$

$$\Delta x_{vi}^{new} = \Delta x_{rv,i}^{new} - \Delta x_{lv,i}^{new} \tag{4.29}$$

where Δx_{vi}^{new} is the change in length of the i^{th} vapor plug, $\Delta x_{rv,i}^{new}$ and $\Delta x_{lv,i}^{new}$ are the changes in location of the ends of the i^{th} vapor plug.

Time step independent of the numerical solution for the model was varied by systematically varying the time step. It was found that varying the time step from 10^{-5} s to 10^{-6} s results in less than 0.2 percent variation in the locations of the liquid slugs. Therefore, the time step used in the numerical solution is 10^{-5} s.

Table 4.1 Initial values of the OCHP

Initial temperature of vapor plugs	$T_{vi} = 35^{\circ}C$
Total length	$L = 0.88$ m
Total number of vapor plugs	3
Total number of liquid slugs	2
Length of each vapor plug	$L_{v1} = L_{v3} = 0.12$ m ; $L_{v2} = 0.24$ m
Length of each liquid slug	$L_{l1} = L_{l2} = 0.2$ m
Wall temperature in cooling section	$T_c = 20^{\circ}C$
Wall temperature in heating section	$T_h = 40^{\circ}C$
Diameter	$d = 0.0015$ m
Total length of heating section	$L_h = 0.44$ m
Total length of cooling section	$L_c = 0.44$ m

4.4 Results and Discussion

The parameters used are listed in Table 4.1. Figure 4.4 shows the variations of pressure and positions of the two ends of the first vapor plug with respect to time. Initially the right end of the first vapor plug is located in the cooling section and condensation takes place. When the pressure is low enough, the adjacent liquid slug starts moving back toward the heating section. As it moves back, the pressure of the first vapor plug increases due to the compression. When the right end moves into the heating section, the condensation ceases. Due to the evaporative of working fluid in the heating section, the pressure of the first vapor plug keeps increasing until the pressure in the first vapor plug is high enough to push the adjacent liquid slug toward the cooling section. This phenomenon repeats itself and periodic oscillation occurs. Fig. 4.4(b) shows the positions of the two ends of the first vapor plug. Since the first vapor plug is located at the end of the OCHP, the left end is always located at $x = 0$ m. The right end oscillates between $x = 0.095$ m and $x = 0.132$ m.

Figure 4.5 shows the variations of pressure and positions of the two ends of the second vapor plug. Since the two ends are free to move into the heating and cooling sections, the amplitude of the oscillation is low. Most of the time when one end is in the heating section the other end would be in the cooling section. This causes the variation in pressure of the second vapor plug smaller than that of the first vapor plug. Figure 4.5(b) shows the positions of the two ends of this vapor plug. The solid and dashed lines represent the location of the right and left ends, respectively. The two ends always move in the same direction, and when one moves into the heating section the other one moves into the cooling section.

Figure 4.6 represents pressure and position variations of the two ends of the third vapor plug with time. The oscillating trends of pressure and positions of the

two ends are the same as those of the first vapor plug and the phase difference is 180^{o}

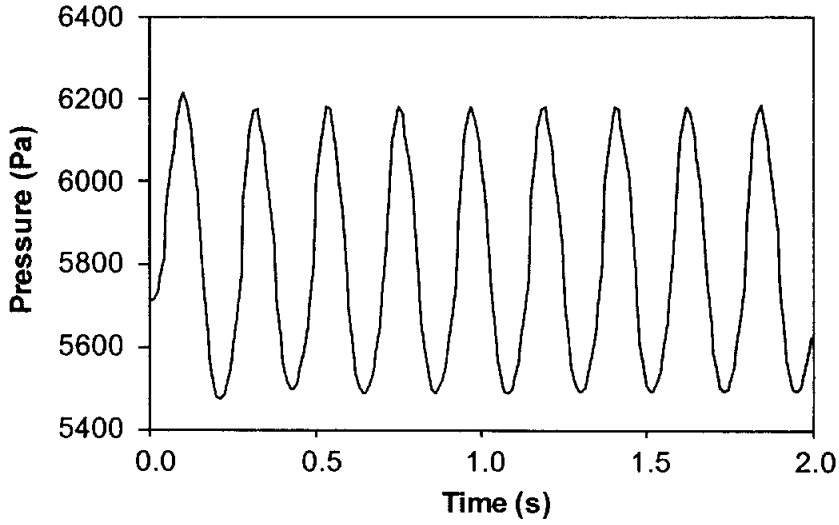

(a)

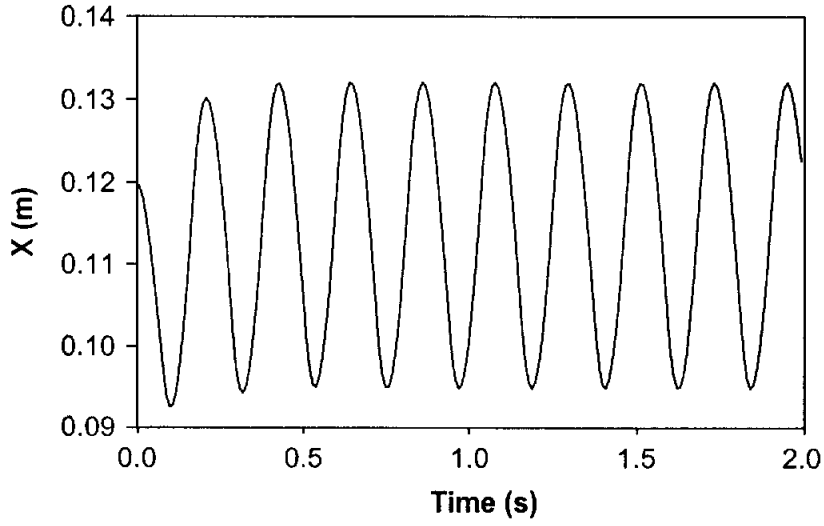

(b)

Fig. 4.4 Variation of pressure and the end positions of the first vapor plug with time

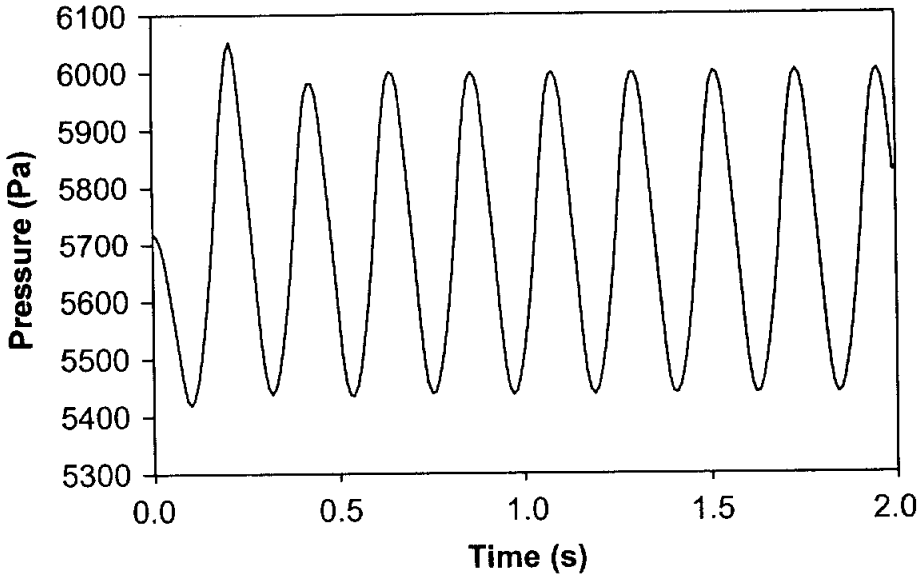

(a)

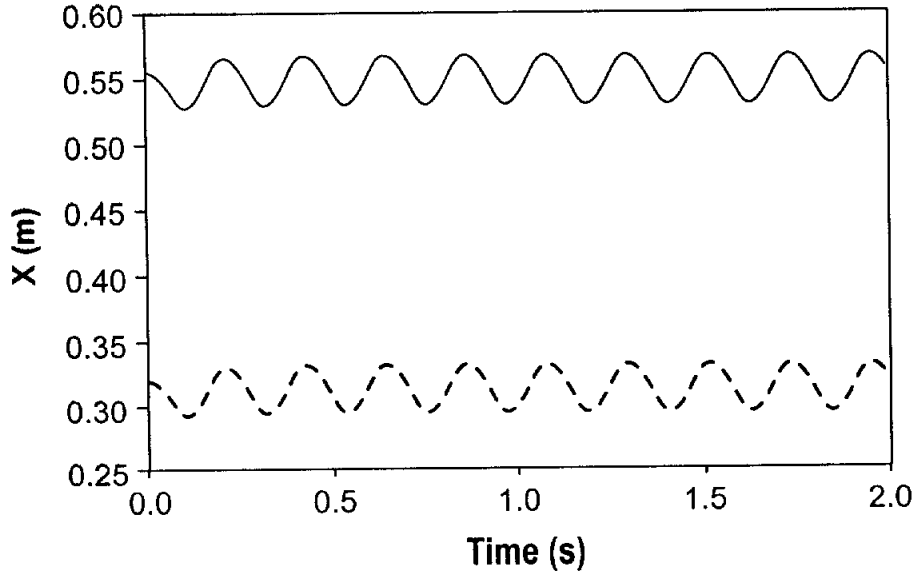

(b)

Fig. 4.5 Variation of pressure and the end positions of the second vapor plug with time

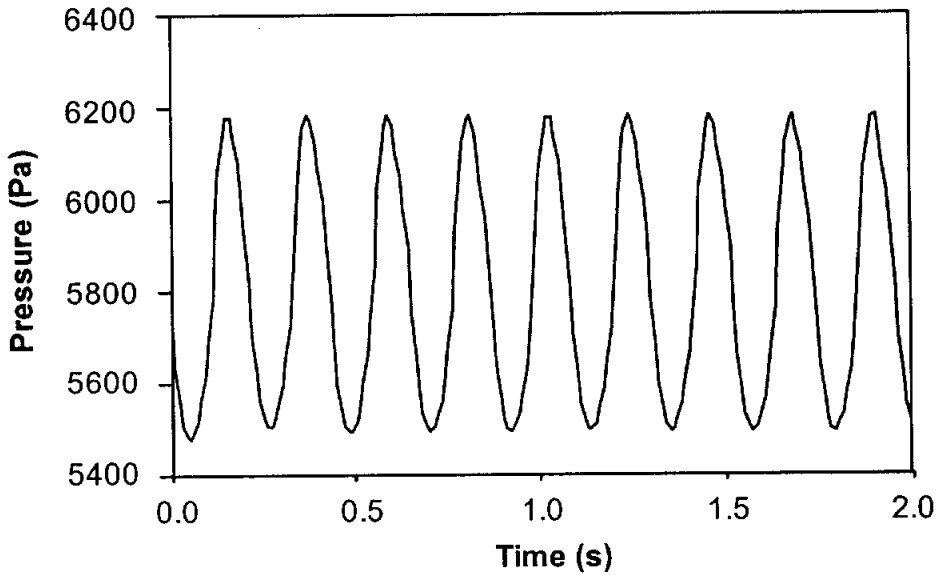

(a)

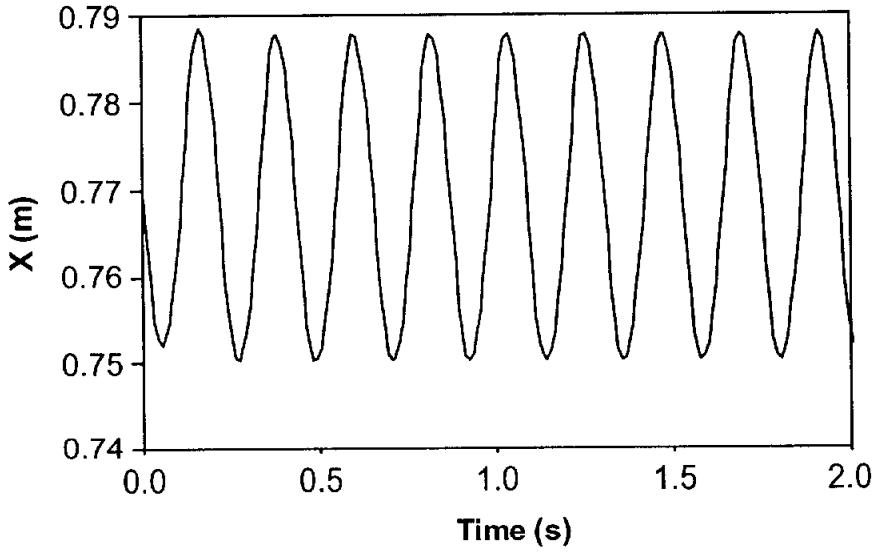

(b)

Fig. 4.6 Variation of pressure and the end positions of the third vapor plug with time

The rate of evaporative and condensation heat transfer of each individual vapor plug, when periodic oscillation is obtained, is shown in Figs. 4.7 ~ 4.9. It can be seen from Fig. 4.7 that when the right end of the first vapor plug moves into the heating section, the evaporative heat transfer increases. When the right end continues moving inside the heating section and compresses the first vapor plug, the evaporative heat transfer increases to its maximal value. As the vapor plug expands, its pressure drops and heat transfer decreases until the right end moves into the cooling section where condensation occurs as well as increasing the condensation heat transfer.

Figure 4.8 shows the rate of the evaporative and condensation heat transfer of the second vapor plug. As mentioned in Fig. 4.5 when one end of the second vapor plug is in the heating section, the other end would be in the cooling section. Therefore, when one end is moving in the heating section, the evaporative heat transfer increases and the condensation heat transfer also increases due to the other end moving in the cooling section.

Figure 4.9 reflects the behaviors of the third vapor plug. It can be seen that the third vapor plug behaves the same as those of the first vapor plug with the phase difference of 180°. The velocity variation with respect to time for each individual liquid slug is shown in Fig. 4.10

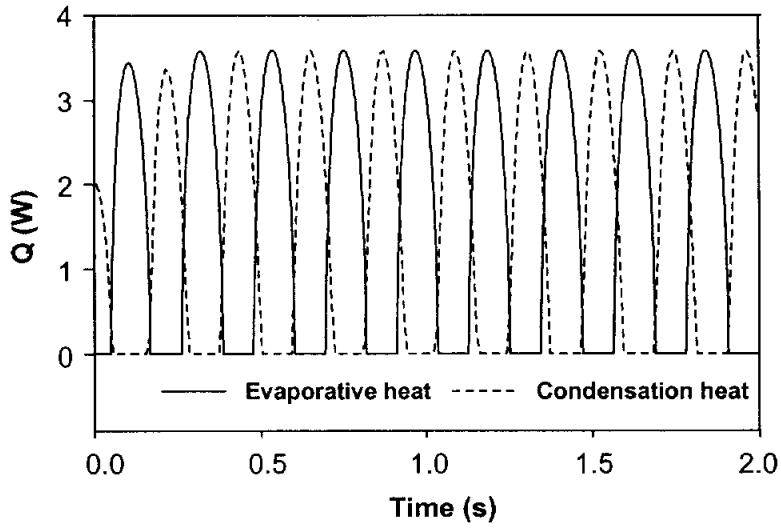

Fig. 4.7 Variation of the evaporative and condensation heat transfer rate of the first vapor plug with time

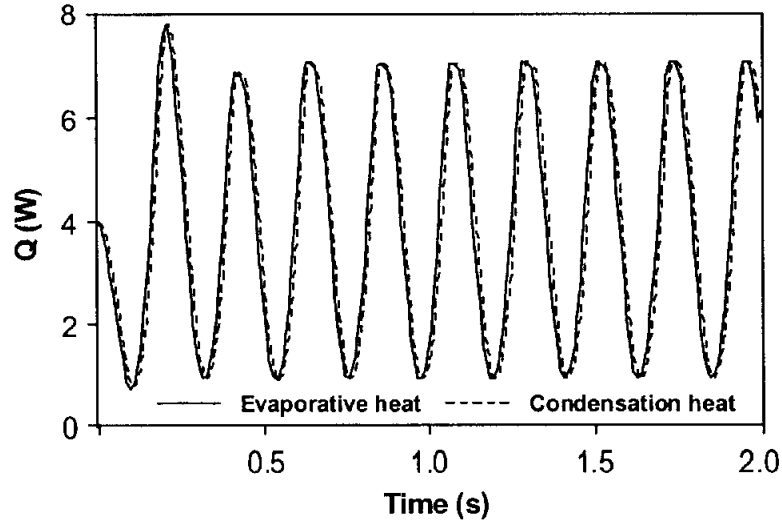

Fig. 4.8 Variation of the evaporative and condensation heat transfer rate of the second vapor plug with time

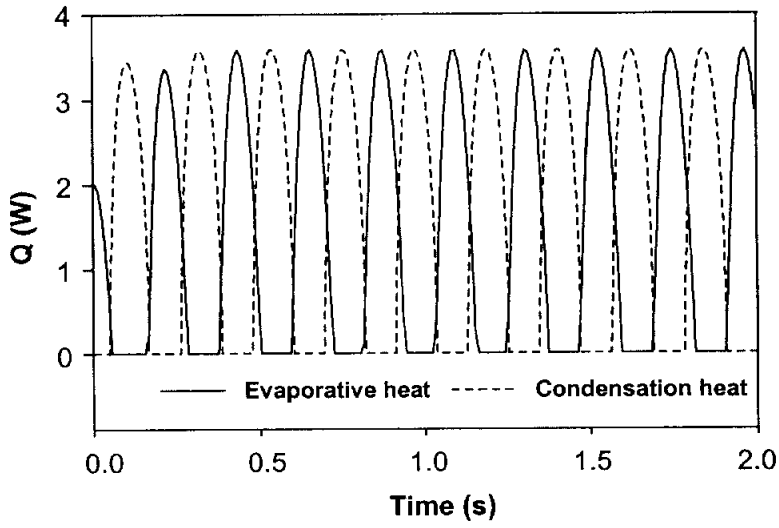

Fig. 4.9 Variation of the evaporative and condensation heat transfer rate of the third vapor plug with time

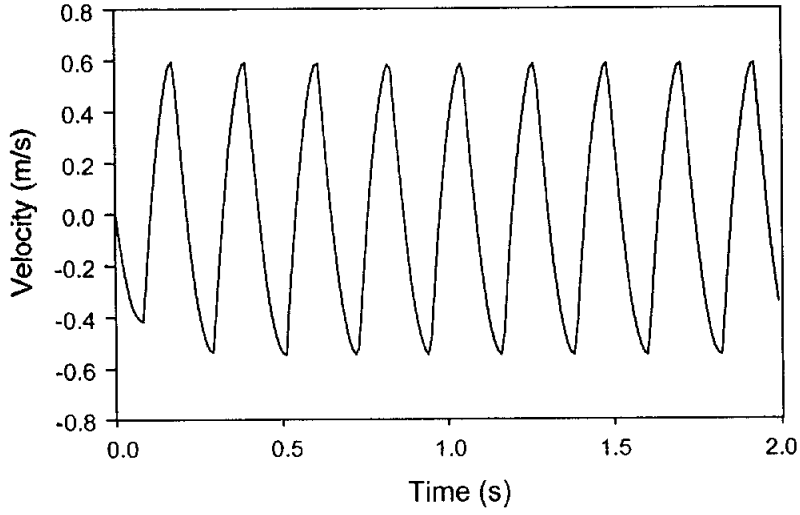

(a) The first liquid slug

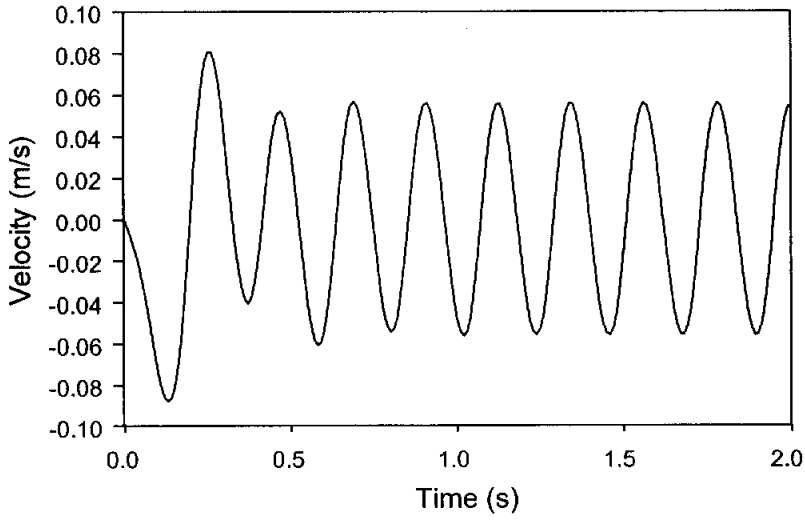

(b) The second liquid slug

Fig. 4.10 Variation of the velocity of each liquid slug with time

To investigate the effect of diameter on the performance of the OCHP, the diameter of the tube is increased to 3 mm. The other parameters and initial values are not changed. Figure 4.11(a) shows the pressure variation with respect to time for the first vapor plug. It can be observed that the frequency of oscillation is lower than that of the small diameter tube. From the Figs. 4.11(b) and 4.11(c) one can conclude that the average temperature of the large diameter tube is lower than that of the small diameter tube. Since the heating area and the temperature difference (between the heating wall section and vapor plugs) of the large diameter tube are greater than that of the small diameter tube, the evaporative heat transfer is higher for the first vapor plug as shown in Fig. 4.12(a). These results are similar for the second and third vapor plugs (Figs 4.12(b) and 4.12(c)).

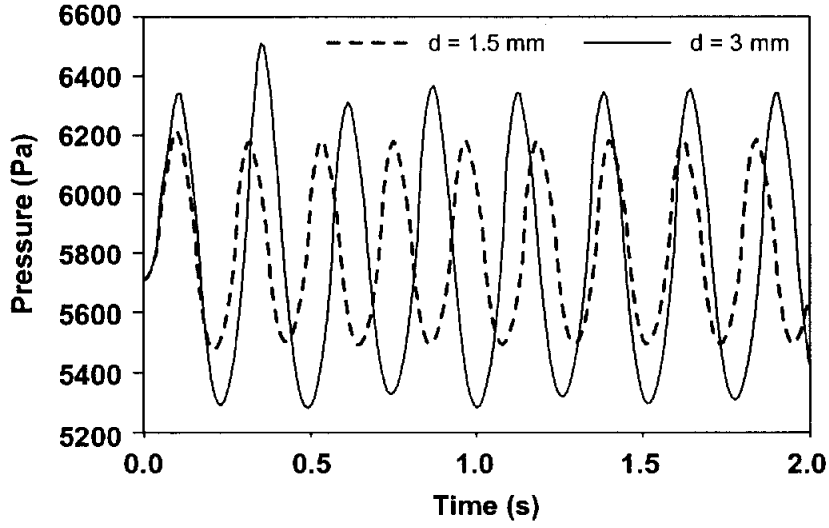
d = 1.5 mm
d = 3 mm
Pressure (Pa)
6600
6400
6200
6000
5800
5600
5400
5200
0.0
0.5
1.0
1.5
2.0
Time (s)

(a)

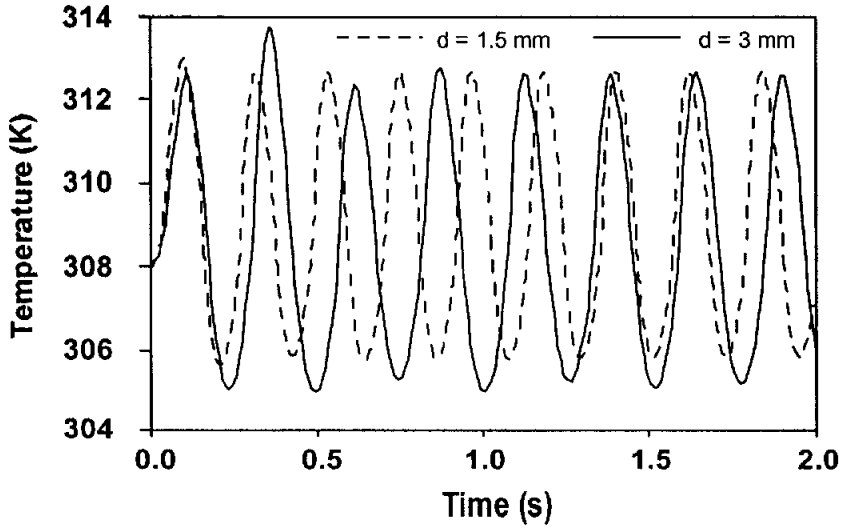
d = 1.5 mm
d = 3 mm
Temperature (K)
314
312
310
308
306
304
0.0
0.5
1.0
1.5
2.0
Time (s)

(b)

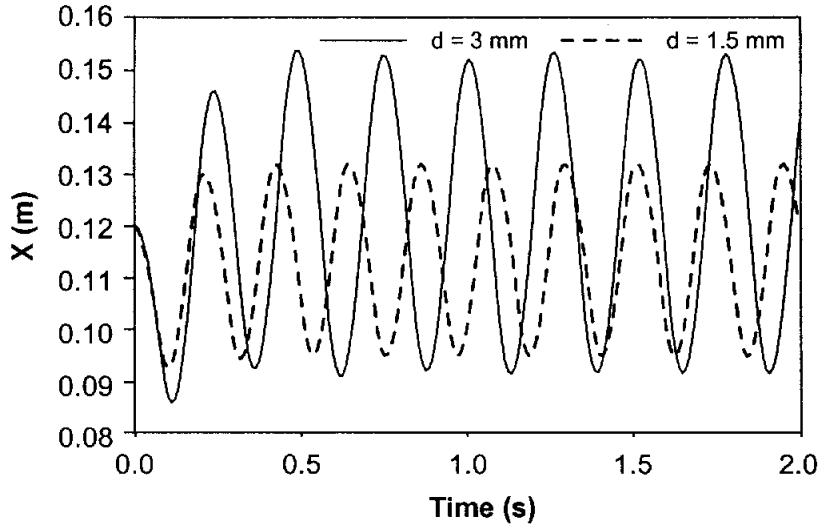

(c)

Fig. 4.11 Effect of diameter on the performance of the first vapor plug

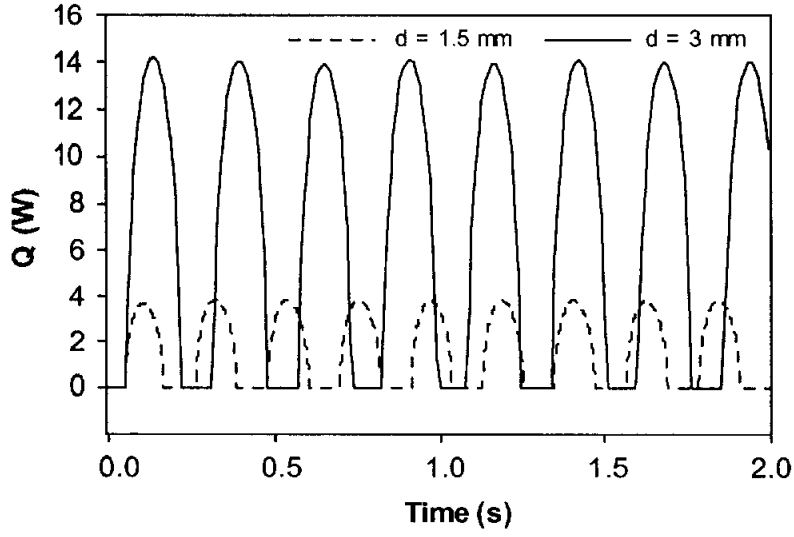

(a) First vapor plug

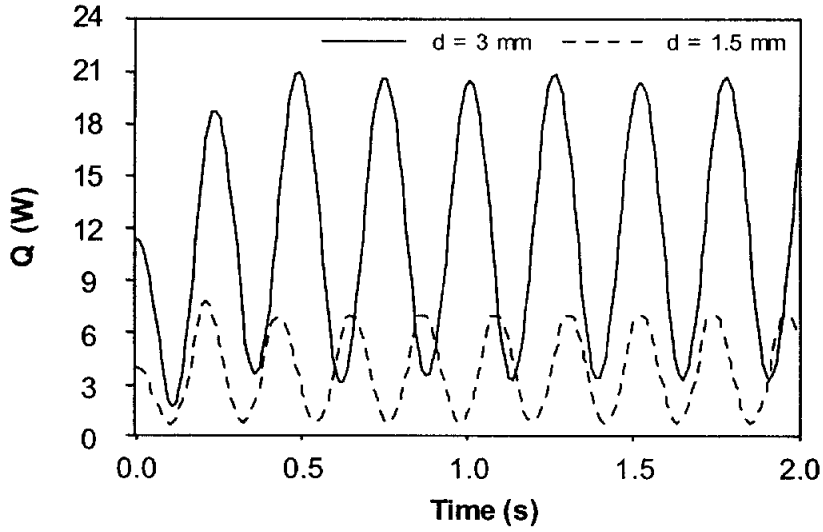

(b) Second vapor plug

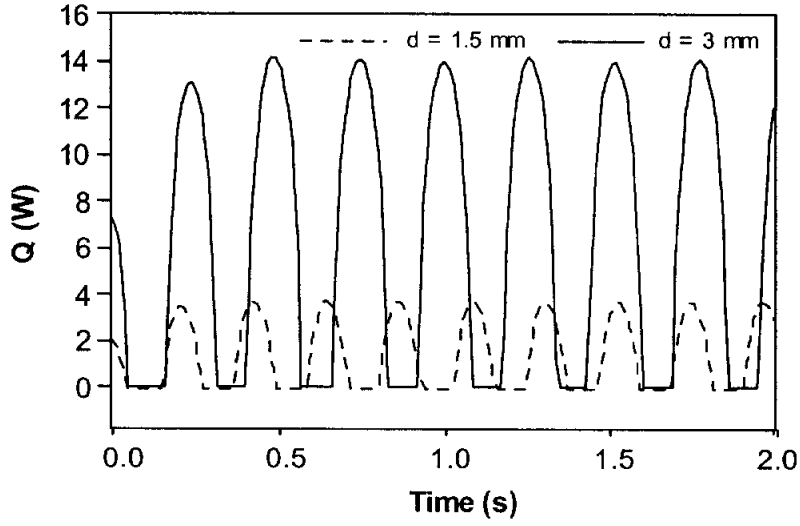

(c) Third vapor plug

Fig. 4.12 Effect of diameter on the evaporative heat transfer rate

The effect of charging ratio on the performance of the OCHP is shown in Fig. 4.13. When the charging ratio is high in the OCHP, the length of the liquid slugs are long, and a higher-pressure difference is needed to move more massive liquid

slugs. Also the amplitude of oscillation increased and the oscillation frequency decreased.

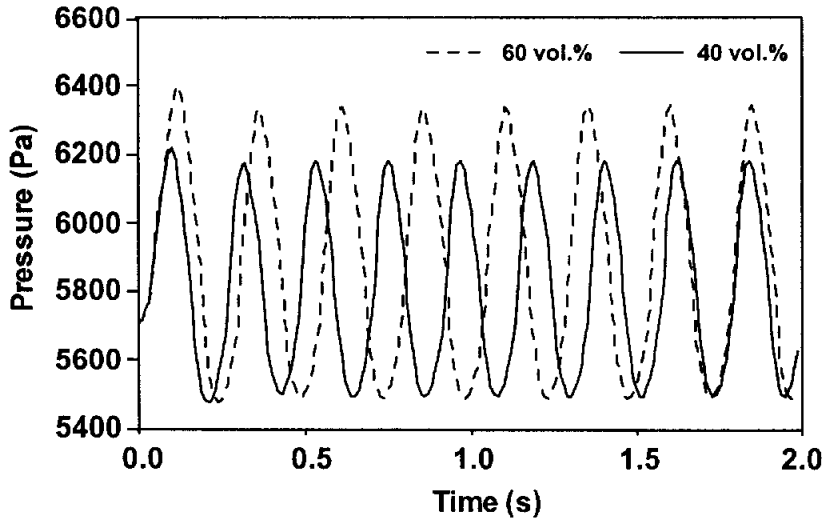

(a) The first vapor plug

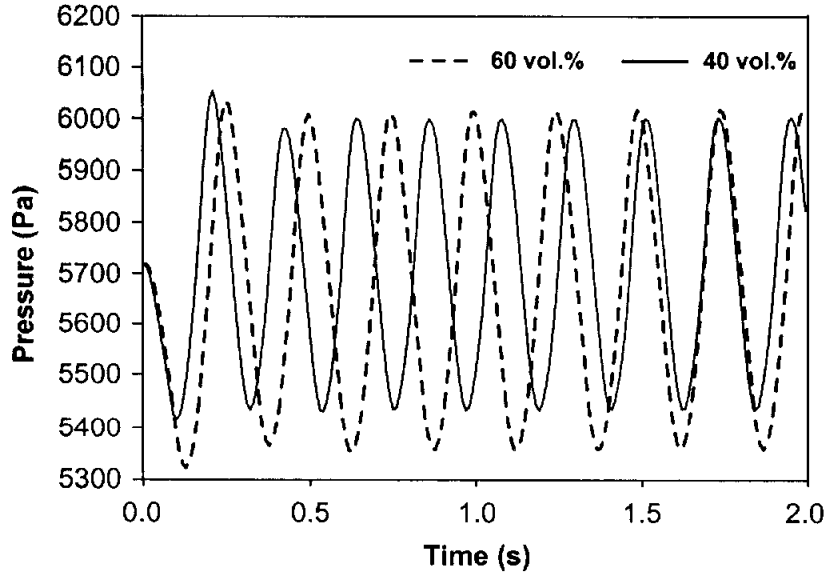

(b) The second vapor plug

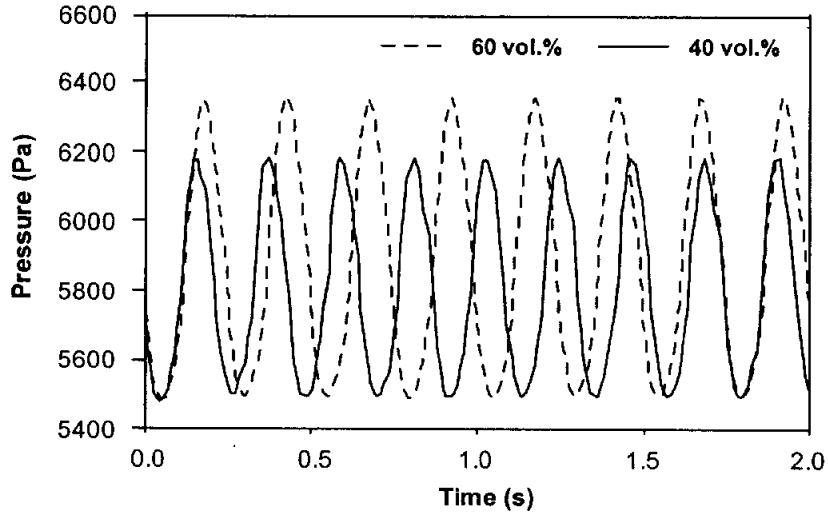

(c) Third vapor plug

Fig. 4.13 Variation of pressure of vapor plugs at different charging ratios

The effect of surface tension on the performance of the OCHP is shown in Fig. 4.14. The amplitude and frequency of oscillation increases for the case with higher surface tension. Since the first vapor plug moves farther into the cooling section (Fig. 4.14(c)), the minimum temperature of the first vapor plug is lower (Fig. 4.14(b)). This may be explained that the working fluid with higher surface tension results in a thinner liquid film. These results are similar for the second and third vapor plug.

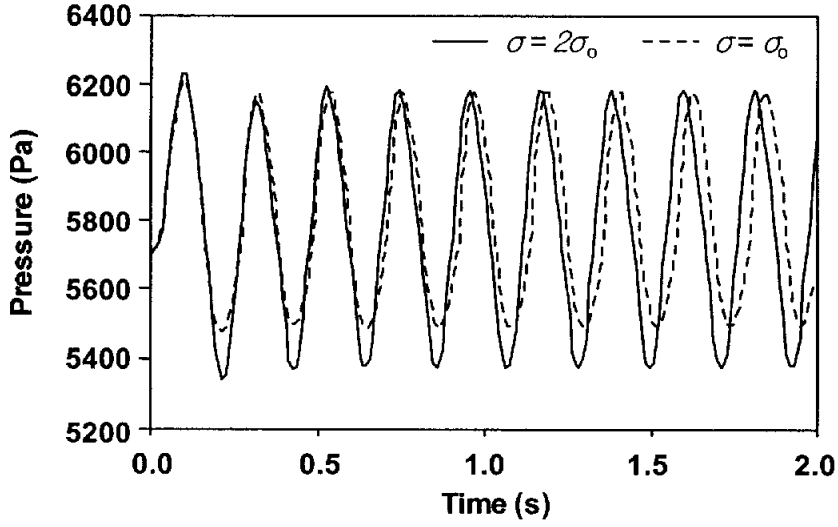
6400
6200
6000
5800
5600
5400
5200
Pressure (Pa)
0.0
0.5
1.0
1.5
2.0
Time (s)
σ = 2σ₀
σ = σ₀

(a)

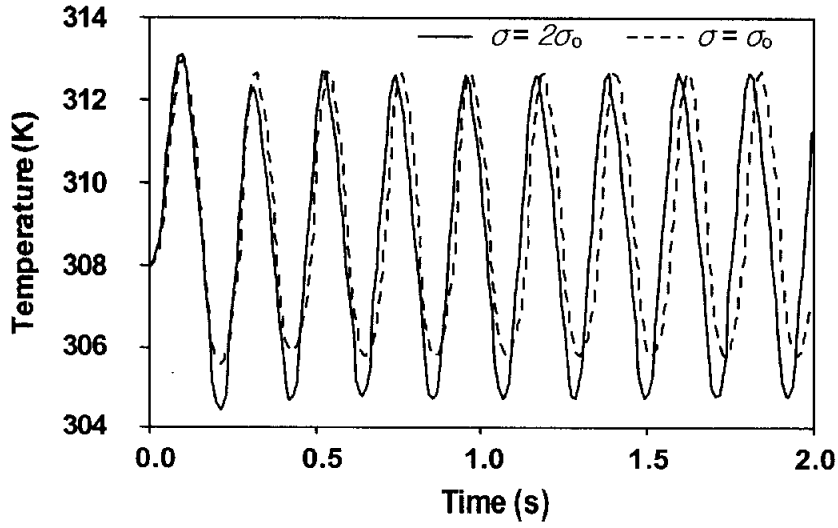
314
312
310
308
306
304
Temperature (K)
0.0
0.5
1.0
1.5
2.0
Time (s)
σ = 2σ₀
σ = σ₀

(b)

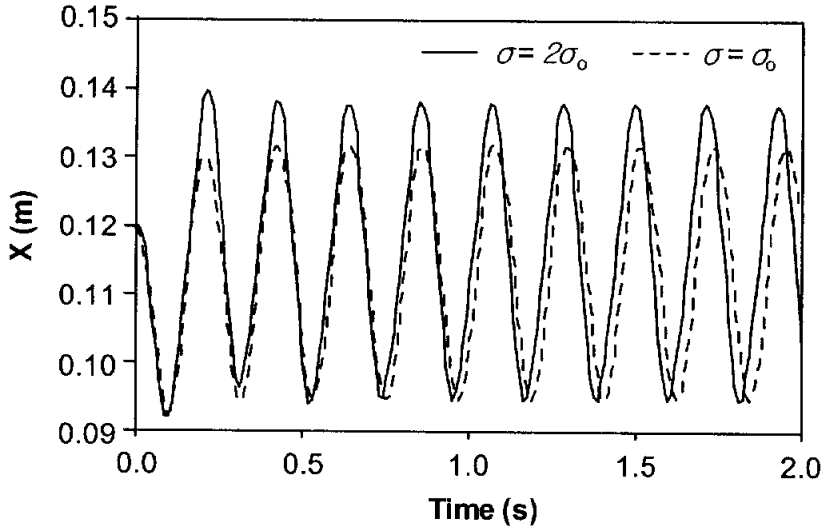

(c)

Fig. 4.14 Effect of surface tension on the performance of the first vapor plug

4.5 Summary

Analytical model of the OCHP with two liquid slugs and three vapor plugs was presented. The behaviors of liquid slugs and vapor plugs in the OCHP were investigated. The following conclusions were obtained.

- The periodic oscillations of liquid slugs and vapor plugs were obtained under specified parameters.
- When the hydraulic diameter of the OCHP was increased to d = 3 mm, the frequency of oscillation decreased.
- By increasing the charging ratio from 40 vol.% to 60 vol.%, the pressure difference between the evaporating section and condensing section increased, the amplitude of oscillation reduced, and the oscillation frequency decreased.
- The working fluid with higher surface tension resulted in an increase in the amplitude and frequency of oscillation. Also the average temperature of vapor plugs decreased.

Chapter 5

Conclusions

The examinations of the operation mechanism of the OCHP using the visualization method revealed that the representative flow pattern in the evaporating section of the OCHP was the oscillation of liquid slugs and vapor plugs based on the homogeneous flow of bubbles generated by nucleate boiling inside liquid slugs and the thin liquid film. The separated flow pattern of short vapor-liquid slug-train units was the flow pattern in the adiabatic section. The movement of working fluid in the OCHP was simulated by two simplified models presented in this study. The first model was based on the homogeneous flow model. The differential equations of two-phase flow were applied and simultaneous non-linear p artial differential equations were solved to predict the oscillating motion of working fluid in the evaporating section of the OCHP. The second model was an analytical model of the OCHP based on the separated flow model with two liquid slugs and three vapor plugs. The governing equations were solved using an explicit finite difference scheme to predict the behavior of vapor plugs and liquid slugs in the adiabatic section of the OCHP.

5.1 Conclusions

The following conclusions were obtained from the results of this study

In the homogeneous flow model

- The oscillation of the mass velocity was steady at the charging ratio of 40 vol.%. The charging ratio of 40 vol.% was predicted as the optimal charging ratio in the operation of the OCHP.
- The dry-out phenomena occurred when the heat flux was increased to 1.5 W/cm^2 at the charging ratio of 40 vol.%.
- The heat flux of 2 W/cm^2 was confirmed as the operation limit of the OCHP due to the dry-out phenomena at the charging ratio of 40 vol.%.
- There was an agreement between the numerical pressure and the experimental pressure data at the heat flux of 1.2 W/cm^2, the charging ratio of 40 vol.%, and the working fluid of R-142b.
- When the hydraulic diameter of the OCHP was increased to 3 mm, the oscillation amplitude of the mass velocity decreased.

In the separated flow model

- The periodic oscillations of liquid slugs and vapor plugs were obtained under specified parameters.
- When the hydraulic diameter of the OCHP was 3 mm, the frequency of oscillation decreased.
- By increasing the charging ratio from 40 vol.% to 60 vol.%, the pressure difference between the evaporating section and condensing section increased, the amplitude of oscillation reduced, and the oscillation frequency decreased.

- The working fluid with higher surface tension resulted in an increase in the amplitude and frequency of oscillation. Also the average temperature of vapor plugs decreased.

The numerical results showed that the proposed models and solution could be used for estimating the operating mechanism in the OCHP.

5.2 Future works

In the future the OCHP will be simulated by combination between the homogeneous model and the separated model.

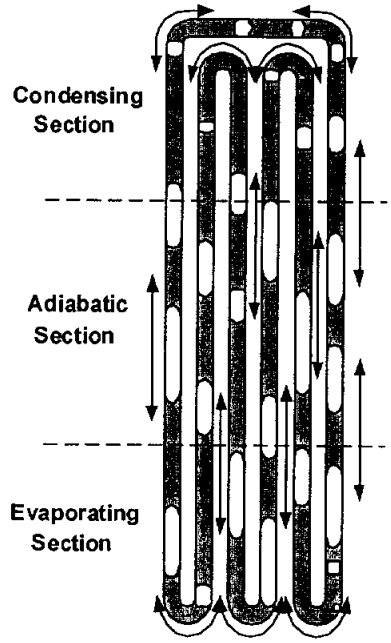

Fig 5.1 Combination model of the OCHP

References

[1] Faghri, A., 1995, *Heat pipe science and technology*, Taylor & Francis, Washington, pp. 625~671, 1~34.

[2] Kurzweg, U. H., and Zhao, L., 1984, "Heat Transfer by High-frequency Oscillations: A New Hydrodynamic technique for achieving large effective thermal conductivities," *Phys. Fluid*, Vol. 27, No. 11, pp. 2624~2627.

[3] Peterson, G. P., 1994, *An introduction to heat pipes*, John wiley & sons, Inc., New York, pp. 4~7, 85~95.

[4] Kobayshi, Y., 1998, "Research and Development of Heat Pipe," *The 2nd Heat Pipe Workshop Korea*, pp. 1~10.

[5] Tong, B. Y., Wong, T. N., and Ooi, K. T., 2001, "Closed-loop Pulsating Heat Pipe," *Applied Thermal Engineering*, pp. 1845~1862.

[6] Akachi, H., 1994, "Loop type serpentine capillary tube heat pipe," *Proceedings of 71th General Meeting Conference of JSME*, Vol. 3 No. 940-10, pp 606~611.

[7] Akachi, H., Polasek, F., and Stulc, P., 1996, "Pulsating heat pipes," *Proceedings of 5th Int. Heat Pipe Symposium*, Melbourne, pp 208~217.

[8] Gi, K., Izumi, T., and Maezawa, S., 1998, "Heat Transfer Characteristics of Looped Oscillating Heat Pipes", *35th National Heat Transfer Symposium of Japan*, pp. 519-520.

[9] Takahashi, O., Kawara, Z., Serizata, A., Kohno, M., Kakinoki, S., and Akachi, H., 1998, "Visualization of Boiling and Condensation in Capillary Tunnel Type Flat Plate Heat Pipe with Proton Radiography," *35th National Heat Transfer Symposium of Japan*, pp 529~530.

[10] Nishio, S., 1997, "Bubble Driven Heat Transport Tubes," *Journal of the Heat Transfer Society of Japan*, Vol. 3 No. 142, pp 53~56.

[11] Hosoda, M., Nishio, S., and Shirakashi, R., 1997, "Bubble-Driven Heat Transport Tube (Flow Pattern and Heat Transport Model)," *34th National Heat Transfer Symposium of Japan*, Vol. 1, pp 267~268.

[12] Numata, S., Shirakashi, R., and Nishio, S., 1999, "Closed-Loop Heat Transport Tube (Effects of Tube Diameter)," *36th National Heat Transfer Symposium of Japan*, pp 675~676.

[13] Gi, K., Sato, F., and Maezawa, S., 1999, "Flow Visualization Experiment on Oscillating Heat Pipe," *36th National Heat Transfer Symposium of Japan*, pp 659~660.

[14] Kim, J. S., Lee, W. H., Lee, J. H., Jung, H. S., Kim, J. H., and Jang, I. S., 1999, "Flow Visualization of Oscillating Capillary Tube Heat Pipe," *Proceeding of Thermal Engineering Conference of KSME*, pp 65~70.

[15] Lee, W. H., Jung, H. S., Kim, J. H., and Kim, J. S., 1999, "Flow Visualization of Oscillating Capillary Tube Heat Pipe," *11th International Heat Pipe Conference*, Tokyo, Japan, Vol. 2, pp 131~136.

[16] Miyazaki, Y., and Arikawa, M., 1999, "Visualization of Oscillating heat pipe," *36th National Heat Transfer Symposium of Japan*, pp 661~662.

[17] Nishio, S., 1998, "Trend of Oscillating Capillary Tube Heat Pipe," *Journal of the Japan Association for Heat Pipes*, Vol. 17, No. 2, pp 8~15.

[18] Nagata, S., Nishio, S., and Shirakashi, R., 1999, "Closed-Loop Heat-Transport Tube," *36th National Heat Transfer Symposium of Japan*, pp. 673~674.

[19] Maezawa, S., 1994, "Capillary Tube Thermosyphon and Dream Pipe," *Proceedings of 71th General Meeting conference of JSME,* Vol. 3, No. 940-10, pp. 593~595.

[20] Gi, K., Sato, F., and Maezawa, S., 1998, "Heat Transfer Characteristics of Double-Ended Closed Oscillating Capillary Tube Heat Pipe," *Journal of JAHP,* Vol. 17, No. 1, pp. 7~11.

[21] Nishio, S., Hosoda, M., Nagata, S., and Watanabe, K., 1997, "Bubble-Driven Heat Transport Tube," *34th National Heat Transfer Symposium of Japan*, Vol. 1, pp. 269~270.

[22] Nagata, S., Takita, Y., Shirakashi, R., and Nishio, S., 1998, "Meandering Closed-Loop Heat-Transport Tube," *35th National Heat Transfer Symposium of Japan*, Vol. 2, pp. 527~528.

[23] Miyazaki, Y., and Akachi, H., 1996, "Heat Transfer Characteristics of Looped Capillary Heat Pipe," *Proceeding of the 5th Int. Heat Pipe Symposium*, Melbourne, pp. 378~383.

[24] Maezawa, S., Nakajima, R., Minamisawa, A., and Gi, K., 1996, "Basic Study on Oscillating Capillary Tube Thermosyphon," *33th National Heat Transfer Symposium of Japan*, pp. 197~198.

[25] Maezawa, S., Izumi, T., Nakazima, R., and Gi, K., 1997, "Nonliner Chaotic

Characteristics of Oscillating Heat Pipe," *34th National Heat Transfer Symposium of Japan*, Vol. 1, pp. 275~276.

[26] Lee, W. H., Kim, J. H., Kim, J. S., and Jang, I. S., 1999, "The Heat Transfer Characteristics of Oscillating Capillary Tube Heat Pipe," *2nd Two-Phase Flow Modelling and Experimentation*, Pisa, Italy, Vol. 3, pp. 1713 ~ 1718.

[27] Lee, W. H., 2000, "Study on Heat Transfer and Flow Characteristics of Oscillating Capillary Tube Heat Pipe", *The doctor degree thesis*, Pukyong National University, Korea.

[28] Miyazaki, Y., and Akachi, H., 1998, "Self-excited Oscillation of Slug Flow in a Micro Channel," *Third International Conference on Multiphase Flow*, Lyon, France, pp. 1 ~ 5.

[29] Miyazaki, Y., Akachi, H., and Arikawa, M., 1998, "Study on Oscillating Heat Pipe", *35th National Heat Transfer Symposium of Japan*, Vol. 1, pp. 531 ~ 532.

[30] Miyazaki, Y., and Arikawa, M., 1999, "Oscillatory Flow in the Oscillating Heat Pipe," *11th International Heat Pipe Conference*, Tokyo, Japan, Vol. 2, pp 143~148.

[31] Maezawa, S. et al, 1996, "Experimental Study on Chaotic Behavior of Thermohydraulic Oscillation in Oscillating Thermosyphon," *5th International Heat Pipe Symposium, Melbourn.*

[32] Maezawa, S., Izumi, T., and Gi, K., 1997, "Experiment Chaos in Oscillating Capillary Tube Heat Pipes," *10th International Heat Pipe Conference, Stuttgart.*

[33] Maezawa, S., Sato, F., and Gi, K., 2000, "Chaotic Dynamics of Looped Oscillating Heat Pipes," *Proceedings of the 6th International Heat Pipe*

Symposium, Chiang Mai, Thailand, pp 404~412.

[34] Dobson, R. T., and Harms, T. M., 1999, "Lumped Parameter Analysis of Closed and Open Oscillatory Heat Pipes," *11th International Heat Pipe Conference*, Japan, Vol. 2, pp. 137~142.

[35] Swanepoel, G., Taylor, A. B., and Dobson, R. T., 2000, "Theoretical Modeling of Pulsating Heat Pipes," *6th International Heat Pipe Symposium, Chiang Mai, Thailand* .

[36] Zhang, Y. and Faghri, A., 2002, "Heat Transfer in a Pulsating Heat Pipe with Open End," *International Journal of Heat and Mass Transfer,* pp. 755~764.

[37] Zhang, Y., Faghri, A., and Shafii, M. B., 2002, "Analysis of Liquid-vapor Pulsating Flow in a U-shaped Miniature Tube," *International Journal of Heat and Mass Transfer,* pp. 2501~2508.

[38] Zuo, Z. J., and North, M. T., "Miniature High Heat Flux Heat Pipes for Cooling of Electronics," *Thermacore Inc., www.thermacore.com.*

[39] Zuo, Z. J., North, M. T., and Ray, L., "Combined Pulsating and Capillary Heat Pipe Mechanism for Cooling of High Heat Flux Electronics," *Thermacore Inc., www.thermacore.com.*

[40] Wong, T. N., Tong, B. Y., Lim, S. M., and Ooi, K. T., 1999, "Theoretical Modelling of Pulsating Heat Pipe," *11th International Heat Pipe Conference*, Japan, Vol. 2, pp. 159~163.

[41] Rossi, L., and Polasek, F., 1999, "Thermal Control of Electronic Equipment by Heat Piped and Two-Phase Thermosyphon," *Proceedings of 11th International Heat Pipe Conference*, Keynote Lecture, Japan.

[42] Suo, M., and Griffith, P., 1964, "Two-Phase Flow in Capillary Tubes," *Journal of Basic engineering, Transaction of the ASME*, pp 576~582.

[43] Mishima, K., and Hibiki, T., 1995, "Effect of Inner Diameter on Some Characteristics of Air-Water Two-Phase Flows in Capillary tubes," *JSME(B)*, Vol. 61 No. 589, pp 99~106.

[44] Kariyasaki, A., Fukano, T., Ousaka, A., and Kagawa, M., 1992, "Isothermal Air-Water Two-Phase Up and Down flows in a Vertical Capillary tube (Ist Report, Flow Pattern and Void Fraction)," *JSME(B)*, Vol. 58 No. 553, pp 40~46.

[45] Fukano, T., Kariyasaki, A., and Kagawa, M., 1990, "Flow Patterns and Pressure Drop in Isothermal Gas-Liquid Concurrent Flow in a Horizontal Capillary Tube," *JSME(B)*, Vol. 56 No. 528, pp 174~182.

[46] Domianides, C. A., and Westwater, J. W., 1988, "Two-Phase Flow Patterns in a Compact Heat Exchanger and in Small Tubes," *Proceedings of second U. H. National Conference on Heat Transfer*, Vol. 11, pp 1257~1268.

[47] Coleman, J. W., and Garimella, S., 1999, "Characteristics of Two-Phase Flow Patterns in a Small Diameter Round and Rectangular Tubes," *Int. J. of Heat and Mass Transfer*, Vol. 42, pp 2869~2881.

[48] Bui, N. H., Kim, J. W., Kim, J. H., Jung, H. S., and Kim, J. S., "Flow Visualization of Oscillation Characteristics of Liquid and Vapor in Oscillating Capillary Tube Heat Pipe," *KSME International Journal*, Vol. 17, No. 6.

[49] Bui, N. H., Kim, J. S., and Jung, H. S., "Theoretical Modeling of Oscillation Characteristics of Oscillating Capillary Tube Heat Pipe," *International Journal of Air-conditioning and Refrigeration,* Vol. 11, No.1, pp 1~9.

[50] Kreyszig, E., 1999, Advanced Engineering Mathematics, *Eighth Edition, John Wiley & Sons, INC.*, pp 541~542.

[51] John, G. C. and John, R. T., 1994, Convective Boiling and Condensation, *Third Edition, Clarendon Press, Oxford*, pp 44~45, 445~447.

[52] Abdul-Razzak, A., Shoukri, M., and Chang, J.S., 1995, "Characteristics of Refrigerant R134a Liquid-vapor Two-phase Flow in Horizontal Pipe," *ASHRAE Transactions Symposium*, pp. 953~964.

[53] Jung, H. S., 2002, "The influence of the flow channel numbers and the heating mode on the heat transfer performance of loop type OCHP," *The master degree thesis*, Pukyong National University, Korea.

[54] Bejan, A., Convection Heat Transfer, 1995, *Second edition, John Wiley & Sons, INC.*, pp 101~102

[55] Alejandro Clausse, "Gas-Liquid Flow and Heat Transfer," *Universidal Nacional del Centro y Comision Nacional de Energia Atomica PLADEMA - Advanced Reactors 7000 Tandil, Agentina.*

[56] Necati Ozisik, M., Finite Difference Methods in Heat Transfer, 1994, *CRC Press, INC.*, pp 100~116

Appendix 1

Effective Thermal Conductivity

The effective thermal conductivity was a representative index to show the performance of heat pipes. The effective thermal conductivity varied according to the working fluid, the charging ratio, the class and shape of heat pipe, the length ratio of the evaporating section and the condensing section, and the inclination angle of heat pipe.

The effective thermal conductivity λ_{eff} is defined as follows:

$$\lambda_{eff} = \frac{LQ}{A(T_{eva} - T_{cond})}$$

where L is the length from the centre of the evaporating section to that of the condensing section, Q is the heat transfer rate from the evaporating section to the condensing section, A is the total cross sectional area of the channels in the OCHP, and T_{eva} and T_{cond} are the mean surface temperatures of the evaporating section and the condensing section, respectively [48].

Appendix 2

Fourth-Order Runge-Kutta

This is one of the popular algorithms for solving ordinary differential equations.

Solve for four different values of $f(t, y)$:

$$k_1 = f(t_n, y_n)$$

$$k_2 = f\left(t_n + \frac{h}{2}, y_n + \frac{h}{2}k_1\right)$$

$$k_3 = f\left(t_n + \frac{h}{2}, y_n + \frac{h}{2}k_2\right)$$

$$k_4 = f(t_n + h, y_n + hk_3)$$

We can then integrate from t_n to $t_n + h$ using:

$$y_{n+1} = y_n + \frac{h}{6}[k_1 + 2k_2 + 2k_3 + k_4]$$

This scheme has a global error of $O(h^4)$ and a local error of $O(h^5)$. We have been able to construct a more accurate approximation of y_{n+1} by sampling the $f(t, y)$ a few times within the interval $[t_n, t_n+h]$.

Appendix 3

Numerical Procedure for the Separated Flow Model

The MATLAB code has been written based on the separated flow model. The code includes three major parts: (1) liquid slug and vapor plug motion, (2) evaporation, and (3) condensation. An explicit finite difference scheme was employed to solve the governing equations of the vapor plug and liquid slug. The time step independent solution of the problem can be obtained when the time step is 10^{-5} s, which is then used in all numerical simulations.

The numerical procedure is outlined as follows. Firstly, initial values such as the initial temperature, length, and end positions (of each vapor plug and liquid slug) are assumed. Then the mass of each vapor plug and liquid slug and the pressure of vapor plugs are calculated. At each time step, the step calculation proceeds for each vapor plug and liquid slug. The new values of pressure at the end of a time step for each vapor plugs are calculated from the change of vapor mass due to evaporation or condensation. The new velocity of each liquid slug is determined from the new value of pressure difference of two adjoining vapor plugs. The new end positions of each vapor plugs are determined by the new positions of liquid slugs. The evaporation and condensation heat transfer for each vapor plug can be calculated and the calculation procedure is repeated.

The flow chart of the numerical analysis for separated flow model is shown in the figure below.

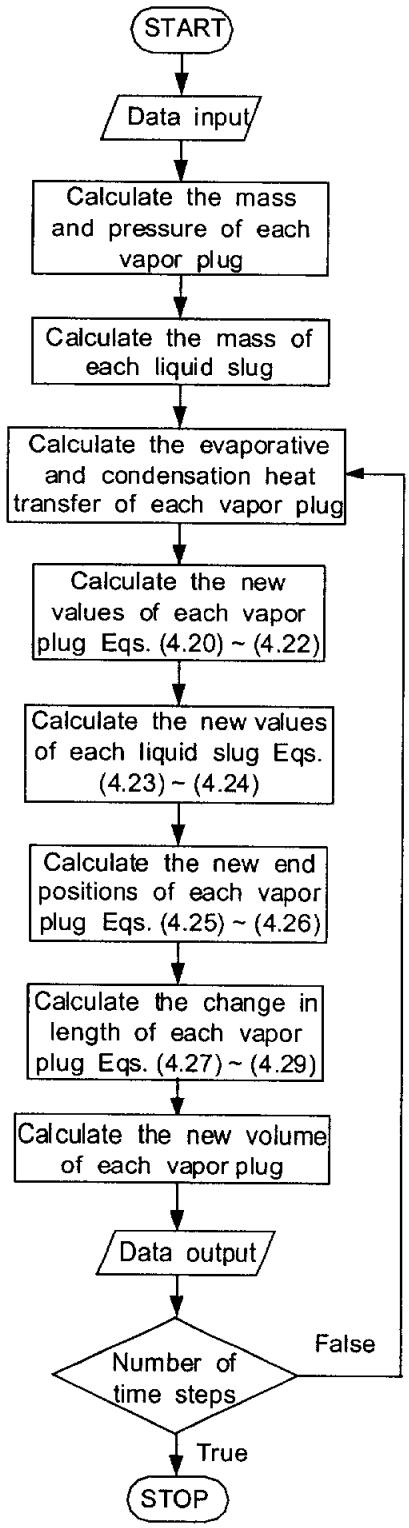
START
Data input
Calculate the mass and pressure of each vapor plug
Calculate the mass of each liquid slug
Calculate the evaporative and condensation heat transfer of each vapor plug
Calculate the new values of each vapor plug Eqs. (4.20) ~ (4.22)
Calculate the new values of each liquid slug Eqs. (4.23) ~ (4.24)
Calculate the new end positions of each vapor plug Eqs. (4.25) ~ (4.26)
Calculate the change in length of each vapor plug Eqs. (4.27) ~ (4.29)
Calculate the new volume of each vapor plug
Data output
Number of time steps
False
True
STOP

Acknowledgments

This dissertation would not have been completed without the help of many people. Especially, I own the greatest debt to Professor Jong-Soo Kim for his financial support, sincere guidance, encouragement and suggestions through the course of this study. I would like to take this opportunity to record my sincere gratefulness to him for his creative influence on my professional activities and for continued warm relationship. I also thank Professor Hoo-Kyu Oh, Professor Young-Soo Kim, Professor Jong-Soo Kum, Professor Eun-Pil Kim, Professor Kwang-Hwang Choi, Professor Suk-Kwon Jung, and Prof. Jeong-Seok Kwon of Department of Refrigeration and Air-Conditioning, Professor Ki-Woo Lee of Korea Institute of Energy Research, Professor Kyu-Il Han, Prof. Sang-Bong Kim and Professor Myung-Suk Lee of Pukyong National University for their many valuable suggestions, advice and kindness.

During the days of working on this study, I have received generous help from all research members of Air Conditioning Lab., including Dr. Wook-Huyn Lee, Dr. Ju-Won Kim, Dr. Jeong-Hoon Kim. I express my sincere thanks to all of them.

Hochiminh City University of Technology has recommended me to The Pukyong National University. I am grateful to Prof. Thanh Ky Tran, Prof. Dinh Tin Hoang, and Prof. Chi Hiep Le for their support and recommendation.

My thanks are also due to my Vietnamese colleagues who have researched and studied in Pukyong National University. In particular, I am grateful to Dr. Tan Tien Nguyen, Ms Tan Tung Phan, Ms Thien Phuc Tran, Ms. Thanh Tong Phan, Ms. Tuong Long Nguyen and Ms. Trong Hieu Bui for their help and advice.

Finally, I would like to thank my parents, sisters, and also my parents-in-law for their great support and encouragement. I express my appreciation to my wife Ba Dieu Uyen Nguyen and my daughter Tuong Nhi Bui and my son Dang Khoa Bui for their continued patience, understanding and endless encouragement.